University of Cape Town

MASTERS THESIS

Studying the southerly eclipsing millisecond pulsar J1748−2446A using MeerKAT

A Masters thesis submitted in partial fulfillment of the requirements for the degree of MSc in Astrophysics and Space Science in the department of Astronomy, University of Cape Town

Author:
Senate P. Lekomola
(LKMSEN001)

Supervisors:
Dr Marisa Geyer
Co-Supervisor:
Dr Robert Main

Abstract

This study focuses on the changes of the dispersion measure (DM), rotation measure (RM) and scattering characteristics of PSR J1748-2446A, a millisecond pulsar in an ablating binary system, as its pulses pass through the companion star's outflow material. To conduct this analysis we used two observations from the South African MeerKAT telescope at L-band frequencies. As PSR J1748-2446A transitions in and out of an eclipse, our observations of its radio emission noted a maximum dispersion measure (DM) increase of $0.089\,\mathrm{pc\,cm^{-3}}$ in Observation 1 and of $0.055\,\mathrm{pc\,cm^{-3}}$ in Observation 2. We record a maximum rotation measure (RM) change of $910 \pm 10\ \mathrm{rad\,m^{-2}}$ in Observation 1 and of $769 \pm 10\ \mathrm{rad\,m^{-2}}$ in Observation 2. We also observe characteristic pulse broadening due to multi-path propagation with an increase in characteristic scattering time (τ) of up to $661.41\,\mu$s in Observation 1 and of up to $36.17\,\mu$s in Observation 2. Given these changes in DM and RM we have estimated the magnetic field strength of the companion's material to be $57 \pm 4\,\mathrm{mG}$ and we have estimated RM values deep into the eclipse to go up to $4100\,\mathrm{rad\,m^{-2}}$. These findings inform us that the companion material is an ionised and turbulent magnetised plasma, with electron densities and density variations much higher than the typical interstellar medium. Furthermore, we investigated the effects of strong lensing induced by this material and discovered ten magnified single pulses with a "signal-to-noise" ratio, SNR > 10.

Dedication

I wholeheartedly dedicate this dissertation to my grandmother,

Patricia Lekomola.

Acknowledgments

First and foremost, I would like to express my deepest gratitude to my primary supervisor, **Dr Marisa Geyer**, for her constant encouragement, patience, and mentorship throughout the course of this research.

I would also like to express my sincere thanks to my co-supervisor, **Dr Robert Main**, for his expertise and advice.

I am profoundly grateful to the **South African Radio Astronomy Observatory (SARAO)** and **National Research Foundation (NRF)** for their financial support and resources.

I would like to express my sincere appreciation to **Prof Matthew Bailes** for his assistance and hospitality during my visit at Swinburne University of Technology.

I would like to thank **Dr Tshiamo Motshegwa** introducing me to this field; it has genuinely improved both my career and personal development.

I would like to extend my heartfelt thanks to **Dr Ceren Ulusoy** for being there the entire time during this journey.

I am also grateful to my peers and the department staff for providing a safe space to work, the environment was a source of motivation.

To my dear friends, words cannot fully express my gratitude for your love, support, and for all those calls at odd hours that meant the world to me.

Lastly, but most importantly, I wish to thank my family for their unwavering love, patience, and prayers. For their sacrifices, their faith in me, and constant support and encouragement when I wanted to give up.

KE A LEBOGA!

Declaration

I know the meaning of plagiarism and declare that all of the work in the dissertation, save for that which is properly acknowledged, is my own.

Signed by candidate

Senate Pearl Lekomola

Contents

1 An introduction to Pulsars **1**
- 1.1 What are pulsars? . . . 1
- 1.2 History of pulsars . . . 3
- 1.3 Pulsar population . . . 5
- 1.4 Globular clusters . . . 6
- 1.5 Spider binaries . . . 6
- 1.6 Terzan 5A . . . 9

2 Propagation through magnetized plasma **10**
- 2.1 Dispersion measure . . . 11
- 2.2 Rotation measure . . . 12
- 2.3 Scattering and scintillation . . . 14
- 2.4 Plasma lensing . . . 15

3 MeerKAT observations **17**
- 3.1 MeerKAT . . . 17
- 3.2 Data recording . . . 18
- 3.3 Observational information . . . 19

4 Methods **22**
- 4.1 Software . . . 22
  - 4.1.1 Pre-processing . . . 22
  - 4.1.2 PSRCHIVE . . . 22
  - 4.1.3 DMfitter . . . 23
- 4.2 Data analysis . . . 23
  - 4.2.1 RFI cleaning . . . 23
  - 4.2.2 Data reduction . . . 23
  - 4.2.3 Improving ephemerides . . . 24
  - 4.2.4 Polarisation calibration . . . 25
  - 4.2.5 Measuring DM and change in DM . . . 26

4.2.6 Measuring RM and change in RM 27

5 Results **29**
5.1 Reference template 29
5.2 DM variations 30
5.3 RM variations 32
5.4 Scattering 33
5.5 DM, RM and scattering relation 33
5.6 Magnetic field 36
5.7 Changes in circular polarisation 38
5.8 Plasma lensing 40

6 Conclusion **41**
6.1 Conclusions 41
6.2 Future work 42

Chapter 1

An introduction to Pulsars

1.1 What are pulsars?

In this thesis I will study a millisecond pulsar in a tight binary system. It is therefore important to first understand what pulsars are, and specifically radio pulsars as observed in this work. Radio pulsars are highly magnetized rotating neutron stars that emit radio emission (Lorimer and Kramer, 2004). They are often called the "clocks of the night" because of the precision of their radio emissions, which are observed to occur at regular intervals, similar to the measured ticking of a clock. This reference to clocks of the night emphasizes the valuable role pulsars play in the field of astronomy by providing reliable cosmic timekeepers.

Neutron stars are extremely dense and compact objects. They possess incredibly strong magnetic fields that are estimated to range from approximately 10^8 Gauss to 10^{15} Gauss (Reisenegger, 2003). When massive stars (of masses $M \geq 10M_\odot$) end their lives in a gravitational collapse, their cores implode, releasing a large amount of energy in the form of a rebound supernova explosion. Some of these supernova remnants form dense objects called a neutron star (Kaspi and Helfand, 2002). Neutron stars are estimated to have a radius of about 10 km and a typical birth mass of about $1.4M_\odot$ (Grinin and Grinin, 2019) which is the Chandrasekhar limit. Named after the Indian-American astrophysicist Subrahmanyan Chandrasekhar, this limit represents the maximum mass that a white dwarf, a remnant of a star's core after it has exhausted its nuclear fuel, can attain while being supported by electron degeneracy pressure (Sreenivasan, 2019). Neutron stars, representing a more extreme collapsed stellar state, are instead supported through neutron degeneracy pressure. With a maximum expected mass of approximately $2M_\odot$, neutron stars are incredibly compact, especially when compared to the Sun's mass (1 $M_\odot$) and radius of about

6.96×10^5 km.

Pulsars are believed to emit radio waves and higher energy emission through two primary processes, namely synchrotron and curvature radiation, although the exact mechanisms remain an area of active research (Lyne and Graham-Smith, 2012). Synchrotron radiation occurs when relativistic charged electrons experience a magnetic force due to their motion in a magnetic field and this force causes them to spiral around the magnetic field lines (Roy and Gangadhara, 2019). As a result of this spiraling motion, they emit radiation across a broad spectrum, ranging from radio waves to X-ray and even gamma-ray frequencies. The spectrum of synchrotron radiation however is not infinitely broad. The highest energy electrons rapidly lose energy, resulting in a cutoff at a specific frequency and a dramatic drop in radiation intensity beyond. Synchrotron radiation is mostly associated with high energy emission, possessing a characteristic power-law spectrum.

Another process of emission is curvature radiation, where relativistic charged electrons are accelerated along the curved magnetic field lines, emitting electromagnetic radiation as a result (Roy and Gangadhara, 2019). Its spectrum is narrower than that of synchrotron radiation. The intensity and the frequency of curvature radiation are determined by the radius of curvature of the accelerated electron trajectory and the energy of the charged electrons.

The radio frequency emission observed from pulsars, represents a small fraction of the total energy budget of a pulsar and is the most poorly understood emission from pulsars. We observe the radio emission of pulsars to be coherent, meaning the radio waves are fully in-phase, leading to the collimated beams of radio waves we detect. Curvature radiation is expected to contribute to these observed properties, and can in particular account for the linear polarization observed in many radio pulsars (e.g. Buschauer and Benford 1976), though complex models to account for all observed properties remain an area of intensive research.

Neutron stars spin rapidly due to the conservation of the angular momentum associated with the originally massive star before its gravitational collapse.. As they spin, they emit radiation beams of coherent radio emission, that sweep across space, much like the beam of a lighthouse sweeps across the sea (see Figure 1.1). When the Earth happens to be in the path of one of these beams, we detect the radiation as a pulse, every time the neutron star rotates with the beam pointing towards us. Hence, the name "pulsar" is derived from the pulsing nature of the radiation we observe. Just as sailors use the periodic beam of a lighthouse to navigate and determine their position, astronomers can use the precise and regular emissions of a pulsar to study the properties of their unique characteristics and to examine the laws of physics under extreme conditions.

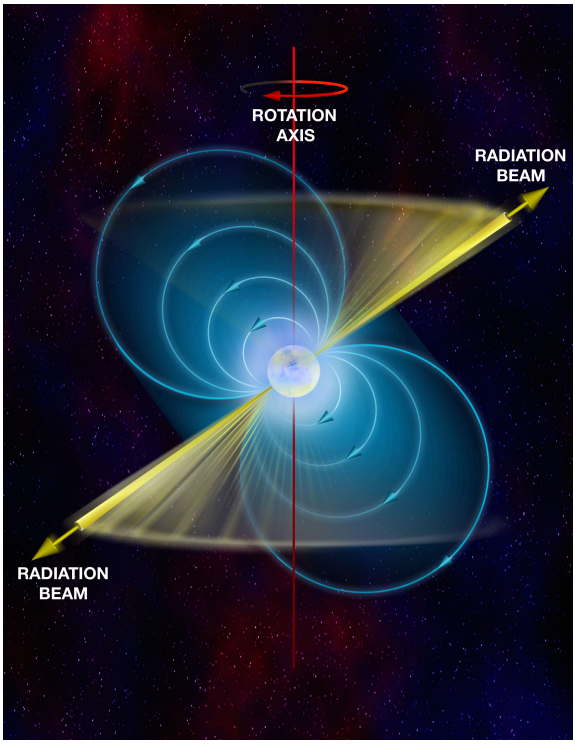

Figure 1.1: Pulsar Emission Mechanism. Pulsars emit radiation beams like a lighthouse's periodic sweep. When Earth intersects the path of these beams along the rotation axis, we observe pulsating radiation. Image credit: NRAO (National Radio Astronomy Observatory).

1.2 History of pulsars

Pulsars were discovered in 1967 by Jocelyn Bell-Burnell and Antony Hewish based at the University of Cambridge in the United Kingdom (Hewish et al., 1968). They serendipitously discovered pulsars while they were observing quasars using the Cambridge radio telescope. They noticed something quite unusual, regular signals, on the data charts which resembled interference or meant possible equipment malfunctions. These regular signals even led to speculations about potential extraterrestrial sources, giving rise to the "Little Green Men" hypothesis. However, as they observed these signals more closely, several characteristics began to stand out. The periodic pulses were stable and when the observed frequency of the pulses was examined, they did not match any man-made sources. Over time researchers began to understand that these were rapidly rotating neutron stars, emitting beams of electromagnetic radiation detectable from Earth. As shown in Figure 1.2, the first to be identified was CP1919 (later designated as PSR B1919+21) which was jokingly nicknamed

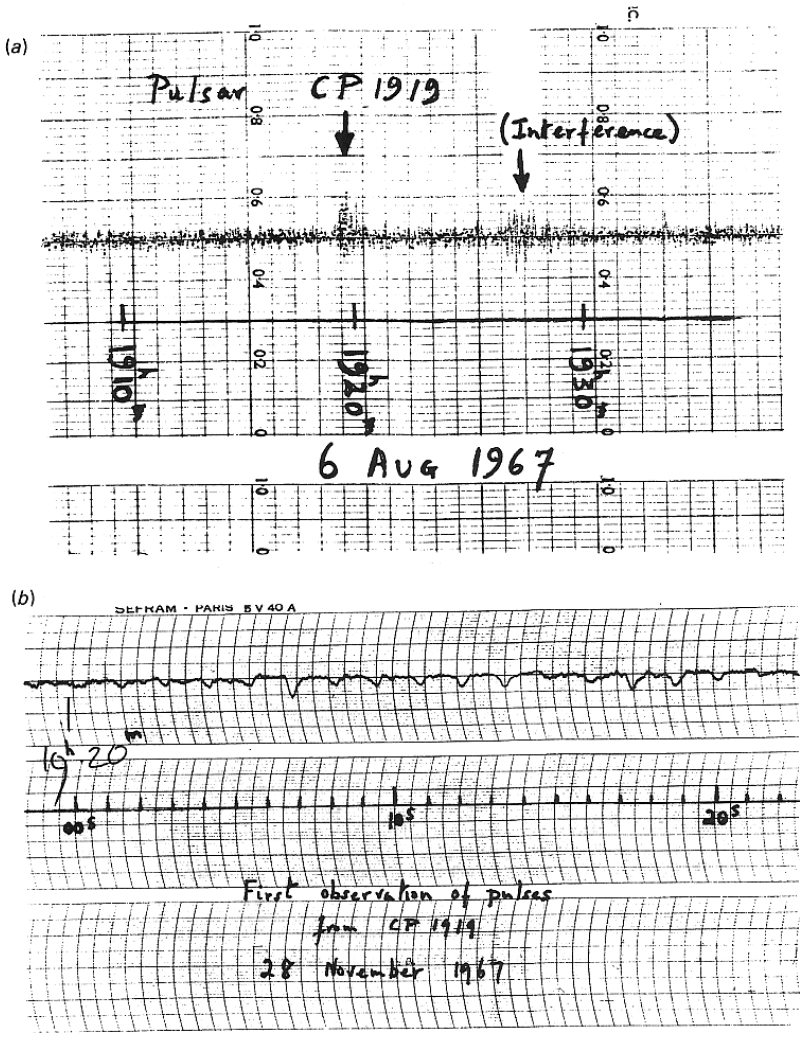

Figure 1.2: The survey chart showing the discovery of the first pulsar. Top: The pulsar CP1919 appears similar to interference on a scintillation survey chart. Bottom: Further observation unveiled its true nature: periodic pulses with a 1.33 s interval, marking the discovery of PSR B1919+21. Image credit: Jocelyn Bell Burnell and Antony Hewish

"LGM-1" for "Little Green Men 1".

1.3 Pulsar population

Over 3,000 [1] pulsars have been identified and catalogued and these are only the pulsars astronomers have detected, Manchester et al. (2005) . There are likely many more pulsars in our Galaxy that remain undetected because they either do not beam their radiation towards Earth or they are too faint or distant to be currently detectable. The exact number of known pulsars is continually increasing as new telescopes are built and current telescopes are improved. The population of pulsars in our galaxy, the Milky Way, is estimated to be about 30 000, but only a fraction, $\sim$200, of these are detectable from Earth due to various factors, including the pulsar's orientation, distance, age, and the surrounding interstellar medium, Lorimer (2012).

Pulsars can be isolated, or found in binaries, with very different properties due to their formation channels.

Isolated pulsars

This category includes typical pulsars, which are typically observed across various parts of the electromagnetic spectrum, such as radio, X-ray, and gamma-ray wavelengths. Younger pulsars within this group are more frequently observed at high-energy wavelengths. The spin periods of these pulsars can range from a few tens to hundreds of milliseconds (Manchester et al., 2005). One notable example is the Crab pulsar, a young pulsar still associated with its supernova remnant, which has a pulse period of 33 ms. MSPs have undergone a "recycling" process, as described below, initially being part of a binary system before evolving into their current isolated state.

Binary pulsars

Pulsars in binary systems are in orbit around another stellar object, such as another neutron star, a white dwarf, or a regular star. This category encompasses a broad range of pulsar rotation periods, from milliseconds to several seconds (Lorimer and Kramer, 2004).

The interaction of a neutron star with a companion star can lead the transfer of angular momentum from the companion star to the neutron star. This results from the companion star overflowing its Roche Lobe, and material falling onto the neutron star thereby increasing the neutron star's spin rate to the millisecond range, ultimately giving birth to a recycled (or spun-up) MSP. This accretion phase of the binary system's evolution is referred to as the Low Mass X-ray Binary (LMXB) phase, (Alpar et al., 1982). Interestingly, some High mass X-ray Binaries (HMXB), in which accretion from a massive stellar companion to the neutron star is driven by

[1] https://www.atnf.csiro.au/research/pulsar/psrcat/

a powerful stellar wind, also lead to X-ray pulsars spinning at millisecond periods, indicating the various evolutionary routes can create rapidly spinning neutron stars.

The vast majority of radio MSPs are in binary systems and have spin periods of just a few milliseconds (<15 ms). MSPs are particularly interesting due to their stability in rotation, making them excellent candidates for precision timing experiments.Their consistent spin rates allow astronomers to use them as precise cosmic clocks, aiding in the study of pulsar orbits, testing the limits of general relativity, and probing the interstellar medium.

1.4 Globular clusters

The subject pulsar of this thesis, PSR J1748−2446A, lives in a well-known globular cluster in our galaxy, called Terzan 5. Globular clusters are densely packed, spherical collections of stars, bound together by gravity. These clusters are so densely packed that they can contain hundreds of thousands, or even millions, of stars. They orbit the cores of galaxies and are typically found in the halo of a galaxy, which is the region surrounding the central disk. Formed in the early stages of galaxy evolution, globular clusters typically consist of older, metal-poor stars, reflecting their ancient beginnings. There are about 157 known globular clusters in the Milky Way galaxy (Harris, 2010). These clusters offer invaluable insights on the initial conditions and chemical makeup of the Universe (Harris, 1996).

The high density of stars in globular clusters increases the chances of interactions between stars. These interactions can lead to the formation of binary systems, where a neutron star can accrete material from its companion as described in the subsection on recycled pulsars above. This accretion process can transfer angular momentum to the neutron star, spinning it up and potentially forming a millisecond pulsar.

Within this diverse range of globular clusters there is one called Terzan 5 which is located in the galactic bulge of the Milky Way as shown in Figure 1.3. Due to its high density of stars, Terzan 5 is home to a large number of MSPs as well as a large number of potential black holes (Heinke et al., 2006). Interestingly Terzan 5 contains a mix of old and young stars, suggesting that it experienced multiple periods of star formation. Terzan 5 is particularly rich in millisecond pulsars, with 39 MSPs identified within it (Ridolfi et al., 2021)

1.5 Spider binaries

Spider binaries are characterized by a rapidly spinning millisecond pulsar paired with a companion star. They are fascinating systems, named after two Australian species

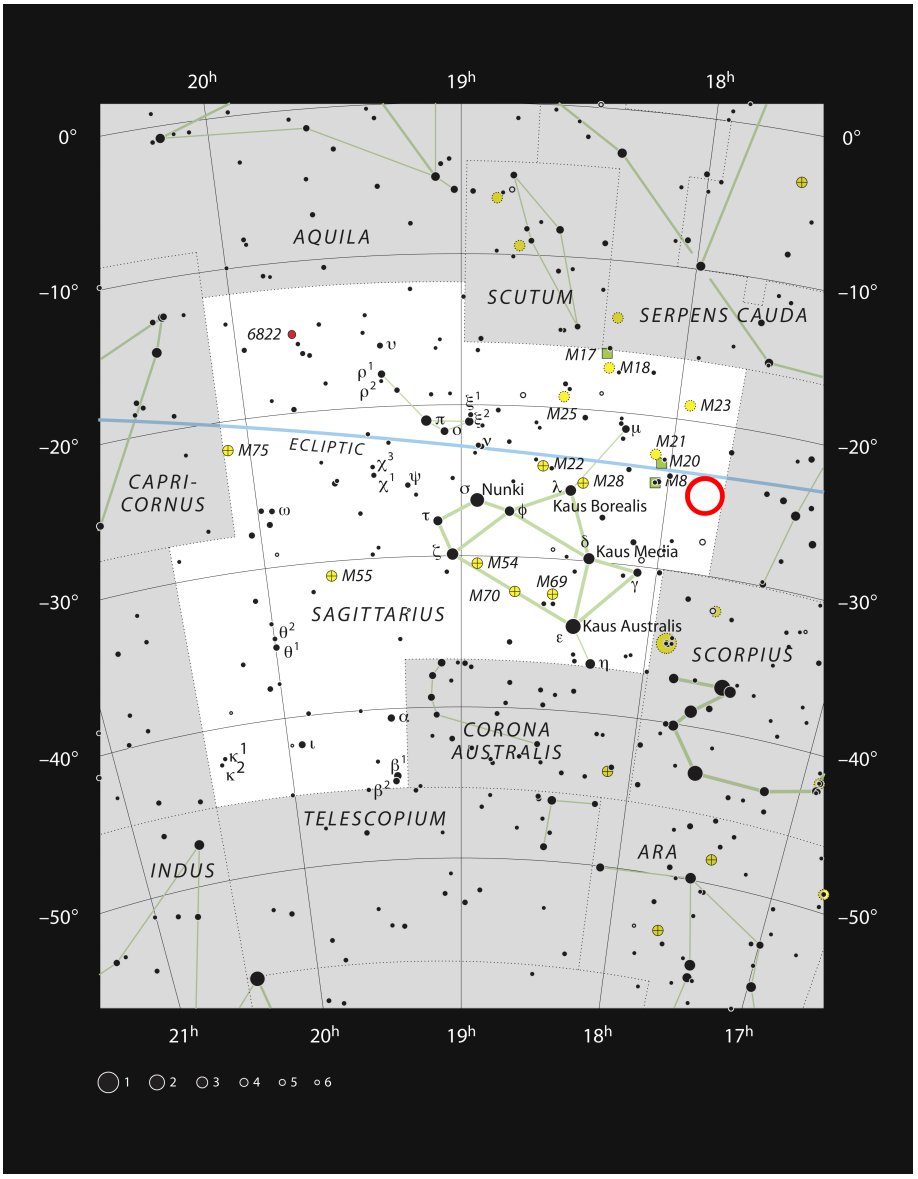

Figure 1.3: Location of Terzan 5. Terzan 5, highlighted here with a red circle, lies within the Sagittarius constellation (white highlighted section), in the Milky Way among other globular clusters and stars visible to the naked eye. Image credit: ESO/IAU and Sky & Telescope.

of spiders, the black widow and the redback, which are known for their unique post-mating behavior where the female devours her male companion. This serves as a cosmic parallel to the pulsar in a spider binary, which through its intense radiation and wind, can ablate and may eventually consume its companion star. Figure 1.4

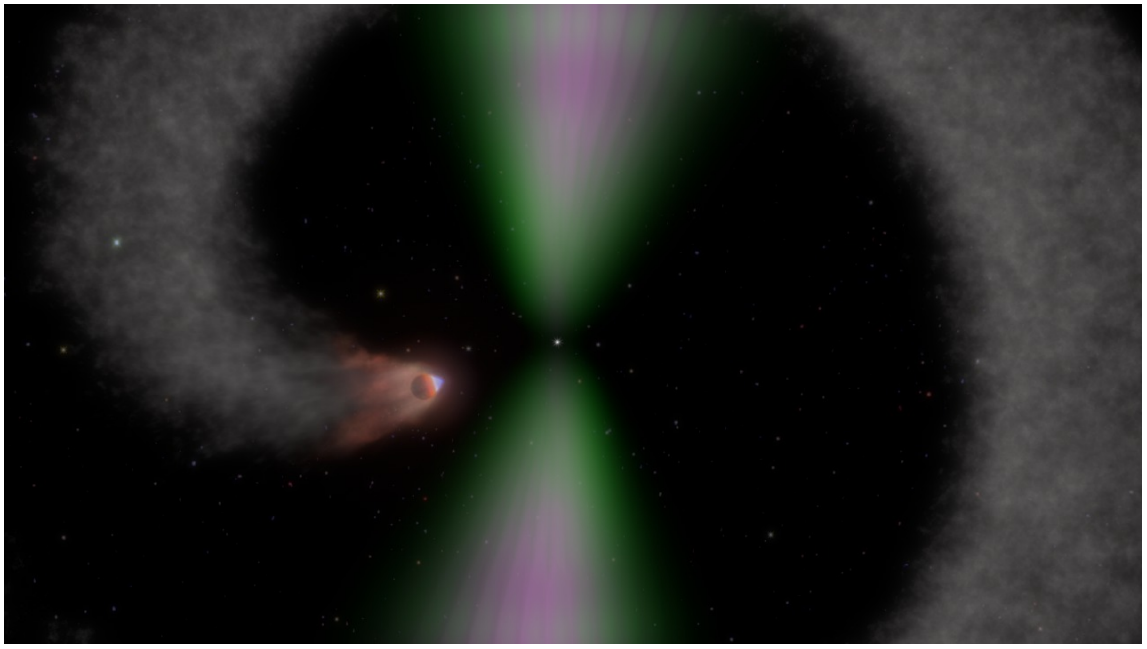

Figure 1.4: An artist impression of a spider binary system. A pulsar blasting the companion stars surface with its intense radiation creating the "cometary tail" of plasma we see. Image credit: NASA's Goddard Space Flight Center

shows an artistic impression of a spider binary system.

Black widow binaries consist of a millisecond pulsar paired with a smaller, lower-mass companion star, typically having a mass equal or less than $0.1M_{\odot}$ (Roberts, 2013). The intense radiation and stellar wind from the pulsar in these binaries are capable of ablating, and potentially, consuming the companion star. On the other hand, redback binaries also feature a millisecond pulsar but a more substantial companion star, generally a main-sequence star with a higher mass ranging between $0.2M_{\odot}$ - $0.4M_{\odot}$ Roberts (2013).The companion star experiences ablation but is not completely consumed, indicating a somewhat more balanced cosmic relationship compared to black widow binaries.

Because of the tight orbital periods, if we observe the binary edge-on or near edge-on, we see the pulsar eclipsed by its companion when the pulsar passes behind the companion or the outflow of the companion. As such spider binaries are pulsar binaries observed as eclipsing systems.

The first such eclipsing system to be discovered was PSR B1957+20 (Fruchter et al., 1988) with a spin period 1.6 ms and an orbital period of 9.17 hrs. Terzan 5A was discovered shortly after (Lyne et al., 1990) and based on its contrasting characteris-

tics to B1957+20, including differing eclipse features and durations, and a different inferred companion mass was labeled as the first redback system.

1.6 Terzan 5A

In this thesis we study this first redback (previously classified as a black widow) eclipsing binary pulsar J1748−2446A (or Terzan 5A abbreviated as Ter5A), formerly known as PSR B1744−24A. The name, J1748−2446A, reflects its position in the sky and follows the naming conventions, the letters and numbers indicate its coordinates in the celestial sphere and in this case, in this case "17:48" refers to the right ascension in hours:minutes, and "-24:46" is a negative declination in degrees:minutes. The "A" at the end distinguishes it from other pulsars with the same coordinates on the sky.

It is a rapidly rotating pulsar with a pulse period of just 11.56 ms (You et al., 2018). It was first observed in November 1989 and again in January 1990 with the 64-m Parkes radio telescope (Lyne et al., 1990). The orbital period of PSR J1748−2446A and its companion is particularly short at only 1.8 hrs, indicating that the two objects are extremely close together with a separation, smaller than the radius of the Sun (1 $R\odot$), of $\sim 0.85 R\odot$. The companion mass is relatively low, estimated to be at least $0.085 M_{\odot}$ (You et al., 2018) , which means that the companion is likely a low-mass star. The binary system shows eclipses, indicating that, as observed from Earth, the companion star periodically obstructs the signal from the pulsar. The system's characteristics make it a great example of a class of eclipsing binary pulsars known as redbacks. PSR J1748−2446A is known for exhibiting eclipses, which is one of the various reasons we are investigating the mechanism and characteristics of these eclipses.

Chapter 2

Propagation through magnetized plasma

Propagating radio waves, such as pulsar emission, are impacted by the presence of ionized and magnetized plasma. Plasma is a state of matter where there are many free charged particles including ions and electrons. It is the electron densities and their variations within plasmas along the line of sight to a pulsar, that causes observational imprints in pulsar data, as described in this chapter.

In the case of a spider binary, such as Terzan 5A, the pulsar emission will encounter and be affected by both (1) plasma from the interstellar medium as well as (2) plasma from the outflow from the companion star.

The interstellar medium (ISM) collectively describes the gas and dust that exist in the space between the star systems in a galaxy. The gas in the ISM is primarily composed of hydrogen and helium, along with trace amounts of heavier elements (Draine, 2011). The ionised component of this ISM, with typical electron densities of $n_e = 0.03\,\mathrm{cm}^{-3}$ and temperatures of approximately 8000 K (Lorimer and Kramer, 2004), that leads to the standard dispersion, Faraday Rotation, scattering and scintillation observed as frequency-dependent effects in most pulsars.

In the case of the dynamic plasma from the companion outflow however, the electron densities will change more rapidly than in the ISM, leading to changes in the plasma's refractive index. The refractive index describes by how much radio waves will slow down as it travels through a medium. We observe these changes in velocity as rapid changes in dispersion and rotation measures, as well as scattering and scintillation described below.

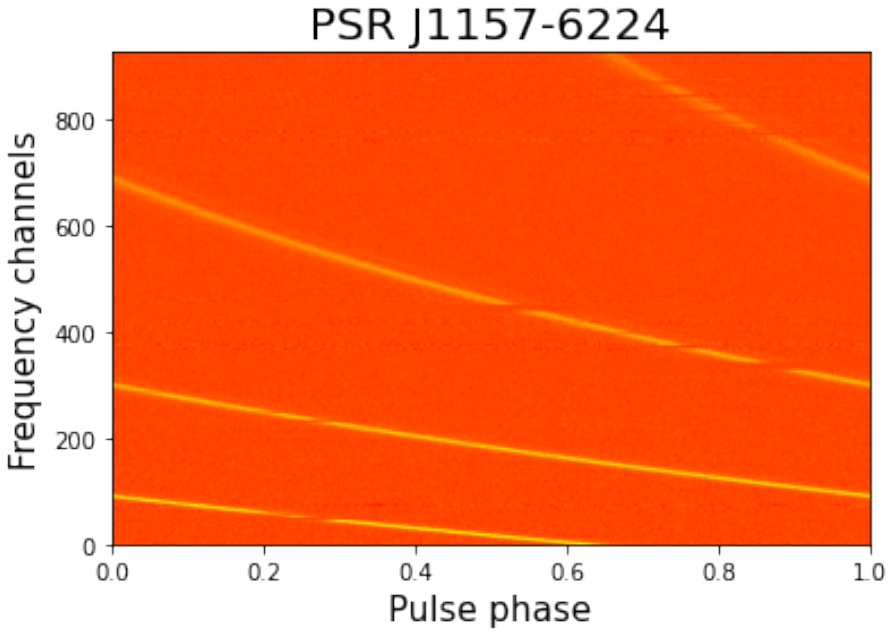

Figure 2.1: Data from PSR J1157−6224 showing a typical pulsar dispersion signature with a DM of 324.35 pc cm^{-3} and a period of 400.522 ms. Pulses at lower frequencies are received later than those at higher frequencies.

2.1 Dispersion measure

When radio waves pass through cold plasma, they experience a delay that depends on their frequency: lower-frequency waves are delayed more than higher-frequency waves, see Figure 2.1. A dispersion measure (DM) correction is used in pulsar observations to account for the time delay experienced by radio pulses as they pass through the plasma. The number of these electrons along the line of sight to a pulsar, integrated from the observer to the pulsar, is quantified by the DM (Lorimer and Kramer, 2004).

The dispersion measure is given in units of parsec per cubic centimeter (pc cm^{-3}), indicating the total column density of free electrons between the observer and the pulsar. The definition of DM in the ISM is:

$$\mathrm{DM} = \int_0^{\mathrm{d}} \mathrm{n_e}\, \mathrm{dl} \tag{2.1}$$

where:

DM- dispersion measure (pc cm^{-3}).

n_e -the electron density in units of electrons per cm^3 along the line of sight.

d- distance from the observer to the pulsar.

The dispersion delay between two frequencies is quantified by the formula, as given by Lorimer and Kramer (2004):

$$\Delta t = 4.15 \times 10^6 \,\mathrm{DM} \left(\frac{1}{\nu_1^2} - \frac{1}{\nu_2^2} \right) \tag{2.2}$$

where:

Δt is the dispersion delay in seconds(s).

DM is the dispersion measure.

ν_1, ν_2 are the two frequencies at which the delay is being measured in megahertz (MHz).

The electron densities in the case of spider binaries, such as Terzan 5A, are not standard and because of this we observe variations in DM. These variations are dominated by the companions outflow especially on short time scales.

2.2 Rotation measure

The rotation measure (RM) describes the amount of Faraday rotation experienced by polarized electromagnetic waves as they propagate through a magnetized plasma. Pulsars emit polarized radio emission. The associated RM is determined by integrating the product of the electron density and the component of the magnetic field along the line of sight over the path of the signal (Lorimer and Kramer, 2004), as shown in Figure 2.2.

Mathematically, this can be written as:

$$\mathrm{RM} = \frac{e^3}{2\pi m^2 c^2} \int_0^d n_e B_{||} \, dl \tag{2.3}$$

where:

RM is the rotation measure in radians per square meter (rad/m^2).

e is the electron charge.

m is the electron mass.

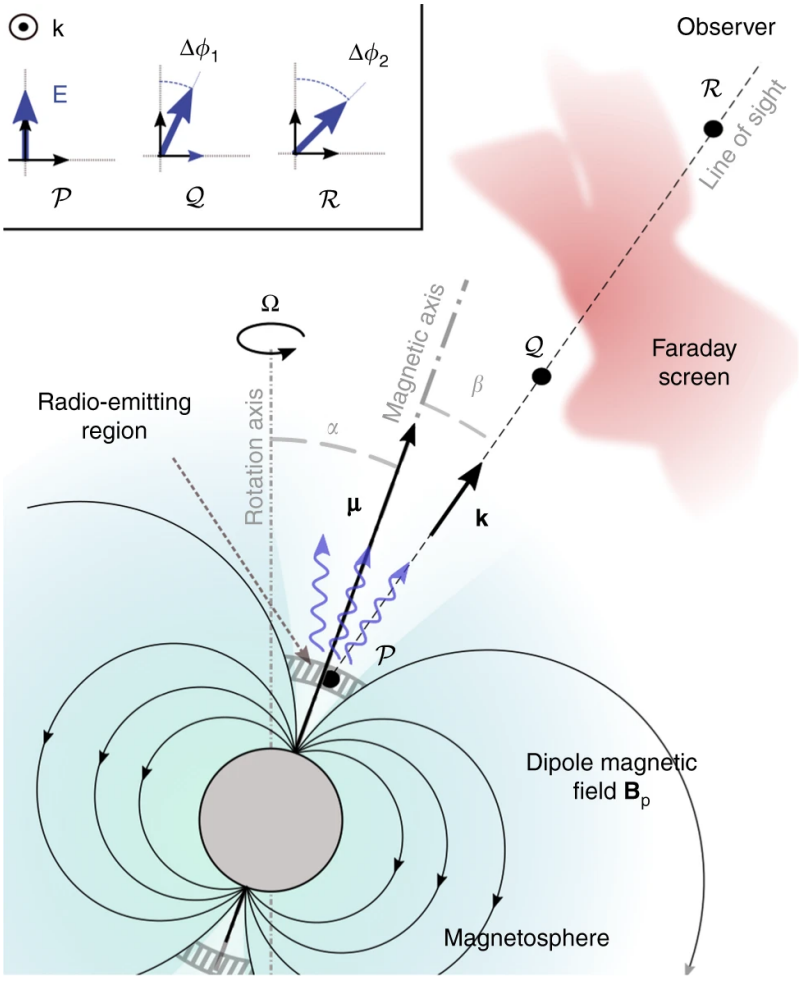

Figure 2.2: RM illustration showing the effect of Faraday Rotation on the polarized waves. As polarized radio waves propagate through a magnetized plasma (Faraday screen) they experience a rotation of the plane of polarization. Image credit: Gueroult et al. (2019)

c is the speed of light.

n_e is the electron density.

$B_{||}$ is the component of the magnetic field parallel to the line of sight.

d is the path length of the pulsar signal through the interstellar medium.

The degree of rotation, $\Delta\theta$, of the plane of polarization at a specific wavelength λ due to Faraday rotation is given by:

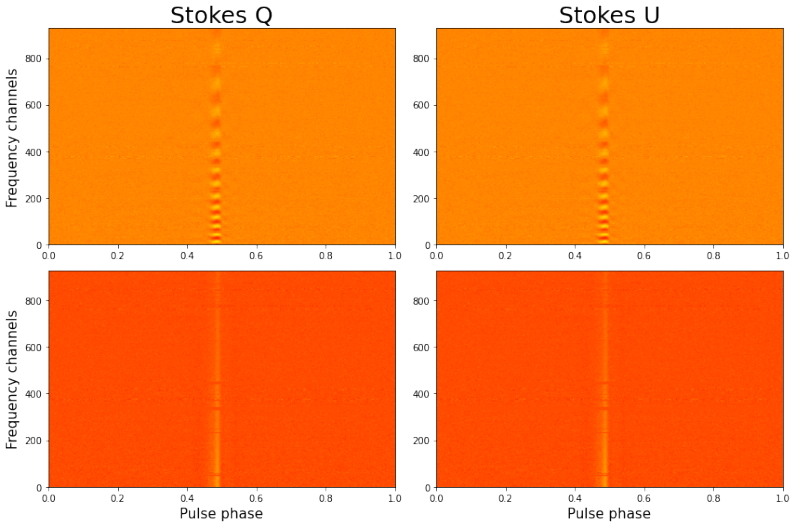

Figure 2.3: Pulsar J1157-6224 RM correction. Top: Variations in the linear polarization before RM correction with the polarization angle changing more rapidly at lower frequency channels due to Faraday rotation. Bottom: After an RM correction of $508\,\mathrm{rad\,m^{-2}}$.

$$\Delta\theta = \mathrm{RM} \times \lambda^2 \tag{2.4}$$

Where:

λ is the wavelength.

RM is the rotation measure.

Since the wavelength is dependent on frequency ($\lambda = \frac{c}{f}$, where c is the speed of light in a vacuum, approximately $3 \times 10^8\,\mathrm{m\,s^{-1}}$), the lower the frequency (that is the longer the wavelength), the more the polarization plane is rotated (Figure 2.3). The amount of rotation experienced by a polarized radio wave is directly proportional to the strength of the magnetic field component along the line of sight. Also the direction of the magnetic field along the line of sight determines the sign of the RM, the magnetic field pointing towards the observer results in a positive RM otherwise a negative RM.

2.3 Scattering and scintillation

Besides dispersion, the intervening plasma can also scatter the radio waves, contributing to the observed pulse broadening. Scattering occurs when radio waves

interact with electron density irregularities and inhomogeneities in the plasma, causing the waves to spread out and travel along different paths (Lorimer and Kramer, 2004). This effect also depends on the frequency of the radio waves, with lower frequencies being affected more. Instead of receiving a sharp, well-defined pulse, we receive a pulse that is asymmetrically broadened with a characteristic scattering tail. A standard pulse shape is convolved with an ISM broadening function, most often modelled as $e^{-\frac{t}{\tau}}$ (Cordes and Rickett, 1998), where τ leads to the asymmetric tail that we observe in Figure 2.4.

Scattering depends more strongly on frequency than dispersion, see Figure 2.4. The pulse broadening time due to scattering, τ, is given by:

$$\tau \propto \nu^{-4} \tag{2.5}$$

Where:

ν is the frequency of observation

Just like how stars appear to twinkle due to Earth's atmosphere, pulsar signals also "twinkle" due to the effects of the intervening plasma. This twinkling is referred to as scintillation.

There are two types of scintillation:

1. Diffractive scintillation: caused by small-scale irregularities in the electron density of the plasma. It results in rapid variations in both time and frequency.
2. Refractive scintillation: caused by larger scale irregularities in the electron density in the plasma. It leads to slower variations in the intensity of the received signal as the path of it is bent (refracted) by the plasma.

Variations in scattering and scintillation can tell us more about the density fluctuations in the plasma they are propagating through. Regions with higher electron densities will, lead to more pronounced scattering and scintillation effects.

2.4 Plasma lensing

As plasma is not homogeneous, radio waves passing through it can get focused or defocused due to irregularities, leading to what is called "plasma lensing". This can lead to temporal magnification or reduction of the pulsar' signal, similar to how a glass lens focuses or defocuses light.

A prominent example of pulse magnification was observed in a spider binary as described in Main et al. (2018), where the lensing events occur during the ingress

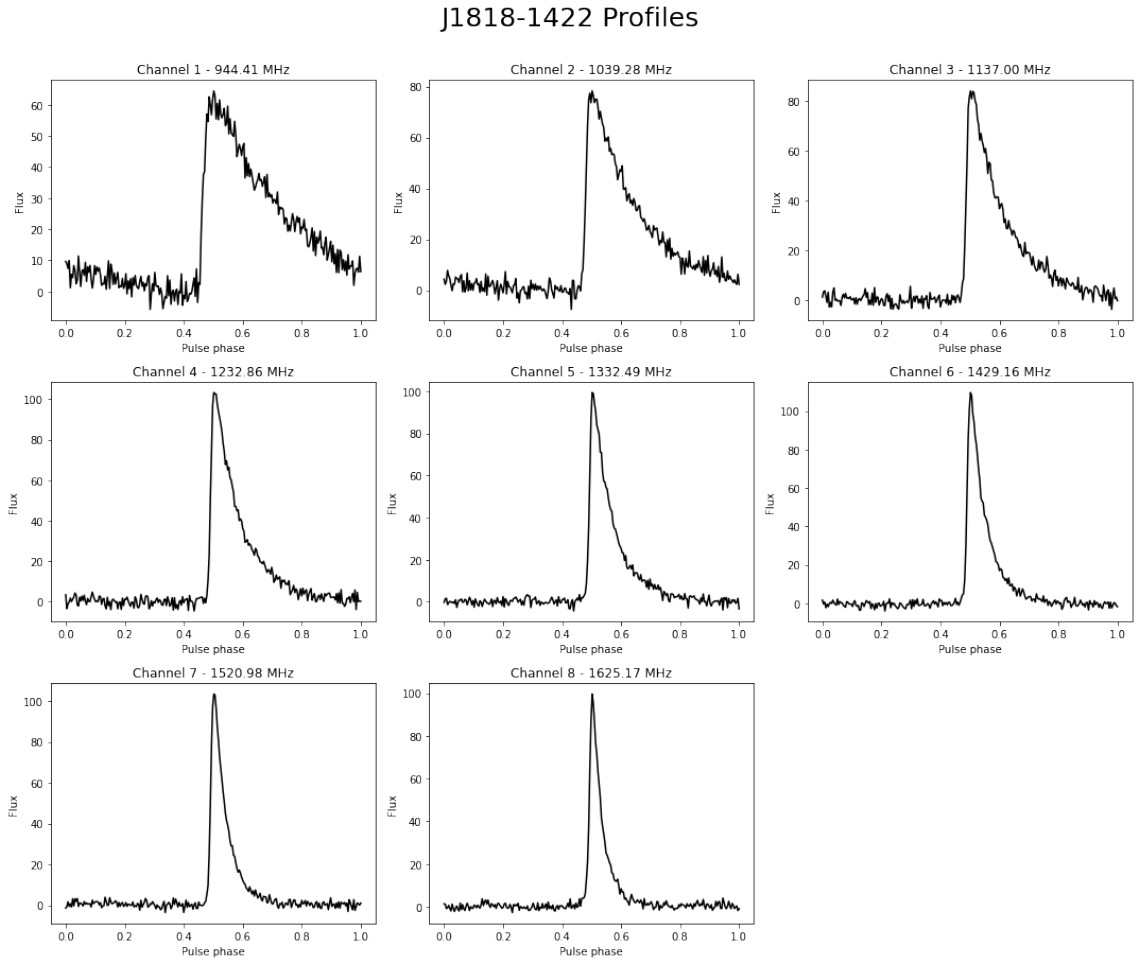

Figure 2.4: Scattering effects as observed in pulsar J1818−1422 at different frequency channels across the MeerKAT L-band. Elongated scattering tails at lower frequency channels, in contrast to the higher frequency channels where they are less extended. These effects can be described by the exponential decay function ($e^{-\frac{t}{\tau}}$).

and egress phases as the pulsar passes behind the companions outflow. The authors observe that in PSR B1957+20 single pulses are magnified by factors of up to 80 times the averaged pulse flux. Observations at different radio frequencies can show different lensing effects. The lensing effects the authors observed are similar to those observed in the repeating fast radio burst, FRB 121102.

Just as a magnifying glass allows you to see details on surfaces (for example jewelry inspection), the companions outflow is acting as a plasma lens allowing us to study the pulsar magnetosphere in more detail.

Chapter 3

MeerKAT observations

3.1 MeerKAT

The MeerKAT radio telescope, located in South Africa, is a precursor to the Square Kilometer Array (SKA) and is one of the most advanced radio telescopes in the world. It operates at radio frequencies, in particular the UHF and L-bands of the electromagnetic spectrum and is particularly well-suited for detailed studies of the Southern Hemisphere sky. The array consists of 64 antennas, each 13.5 meters in diameter, working together as an interferometer to create high-resolution images as well as high time resolution data (Bailes et al., 2020).

The MeerKAT antennas adopt an unshaped "feed down" offset Gregorian design, allowing for the integration of multiple receiver systems (Figure 3.1). The L-band observations, as used in this work, spanning a frequency range of 856 MHz - 1712 MHz, yield a system equivalent flux density (SEFD) of approximately 7 Jy when averaged across this band (Camilo et al., 2018). This level of sensitivity allows for detection of relatively weak emissions.

The MeerKAT radio telescope is engaged in various projects, each addressing different subfields within astronomy, therefore contributing to a wide range of astronomical research. The telescope is also particularly well-suited to conducting radio pulsar science, with an approximately 5-fold increase in sensitivity over the well-known Parkes telescope.

The largest pulsar project is MeerTime, which is a 5 year program focusing on regularly timing over 1000 radio pulsars. The research focuses of the MeerTime project includes investigating the internal composition of neutron stars through pulsar timing, to understand how binary pulsars originated and how they change over time, to

search for gravitational waves using pulsar timing arrays, to provide insights into relativistic gravity, and to monitor radio magnetars and pulsar populations in globular clusters (Bailes et al., 2016).

MeerTime also shares data with scientists from around the world to contribute their expertise and insights. I was one of the lucky recipients of this data and as a beneficiary this data, my thesis is poised to make contributions to our understanding of the eclipsing nature of Terzan 5A.

3.2 Data recording

Data for the MeerTime project described above can be recorded in two modes using the PTUSE (Pulsar Timing User Supplied Equipment) back-ends, namely *fold-mode* and *search-mode* (or single pulse mode) (Bailes et al., 2020).

Fold-mode data is used to observe well-known pulsars. By using up-to-date ephemerides or timing model for these sources, the recording backend folds the time series data using the known pulse period (and other timing parameters) to produce data with a time-resolution of 8 s per data chunk, and with 1024 phase bins across the pulse profile. As part of the data capturing process the dispersion (as described in Section 2.1) is also removed via a process known as coherent dedispersion.

Search mode data, on the other hand, retains a much higher time resolution data product for the pulsars observed, such that during analysis researchers are able to study single pulses of the observed pulsar. This observing mode is also very well suited to studying globular clusters as it allows you to study several pulsars in the globular cluster that all fall into the MeerKAT primary beam from the same data set. By simplify folding (reducing) the data using different folding emphemerides, pulse profiles of a range of pulsars within the primary beam can be formed.

In this thesis we make use of Terzan 5 search-mode (single pulse) data that were recorded as part of the MeerTime research sub-theme that focuses on studying Globular Clusters (PIs: Scott Ransom and Andrea Possenti; www.meertime.org).

During the observations the MeerKAT beam was centered on PSR J1748−2446N (2019 data) and J1748−2446O (2020 data). These original data sets have a native time resolution of 9.57 μs and 4096 frequency channels. In the post-processing we refold this data using the best-known ephemerides of PSR J1748−2446A to obtain pulse profiles PSR J1748−2446A. The refolding was done using `dspsr` (see Section 4.1) and produced data with 8 s time resolution, 768 (2019 data) or 1024 (2020 data) frequency channels and 1024 phase bins across a pulse profile as described next. For all our data we retained polarisation information for our subsequent analysis.

3.3 Observational information

In this research, we will examine the data from pulsar J1748-2446A, focusing on the diverse characteristics of its pulse emissions. This information was collected during two separate observations on 2019-05-27 (Observation 1) and 2020-02-27 (Observation 2) as shown in Table 3.1. The observations are divided into pulse phase bins to construct a detailed profile of the pulsar's emission over a single rotation. In Observation 1 we observed the pulsar for 9002 s and in Observation 2 for 12593 s. Since our orbital period is 6480 s we observe our pulsar for more than a full orbit. In Observation 1 we see the pulsar for about 70% of the pulsar orbit and we observe the pulse broadening during the eclipse egress, see Figure 3.2. In Observation 2 we see the pulsar for only about 30% of the pulsar orbit and unlike Observation 1 we observe mini eclipses in between the pulsar's emission and we see some detection during the eclipse, see Figure 3.3. The data spans multiple frequency channels and includes four polarization states. The observations have been parsed into smaller segments, subintegrations, for detailed analysis. Table 3.1 below also contains the best known dispersion measure, rotation measure and epoch of periastron of our datasets. In binary systems the term "periastron" refers to the point in the pulsar's orbit when it is closest to its companion star. The "Epoch of periastron", T0, is the time when the pulsar last passed through the periastron.

Table 3.1: MeerKAT observations of PSR J1748−2446A used in this thesis. The DM and RM values presented here are the reference header values for each observation.

Description	**Observation 1 2019-05-27**	**Observation 2 2020-02-27**
Number of pulse phase bins	1024	1024
Number of frequency channels	768	1024
Number of polarizations	4	4
Number of subintegrations	1126	1576
Observation duration (s)	9002	12593
Dispersion measure ($\mathrm{pc\,cm^{-3}}$)	242.342	242.342
Rotation measure ($\mathrm{rad\,m^{-2}}$)	180	180
T0: Epoch of periastron (MJD)	58500.4861241885	58500.4861241885

Figure 3.1: The MeerKAT Telescope unveiled on the 13th July 2018 by the former Deputy President of South Africa, Mr David Mabuza . The MeerKAT telescope is a 64-dish radio interferometer located in the Northern Cape of South Africa Image Credit: SARAO (2018)

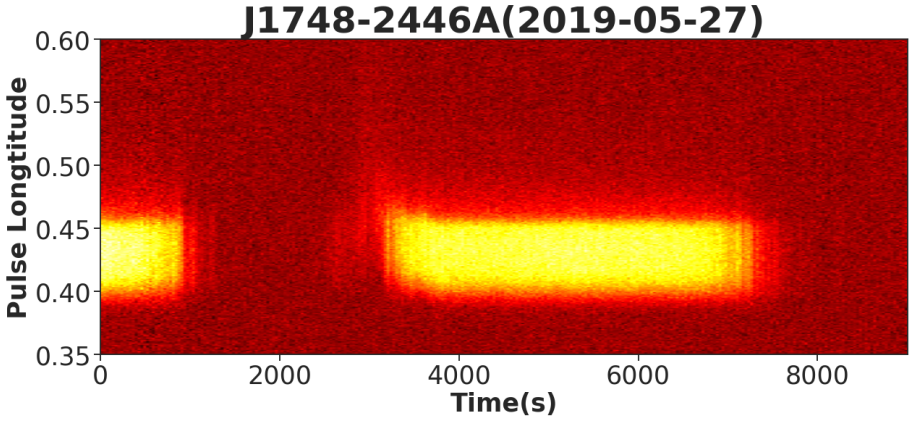

Figure 3.2: Observation 1 data showing pulse longitude over 9002 s ($\sim$ 1.4 orbits) of the PSR J1748−2446A binary. We have zoomed in on the pulse longitude and observe the pulse being delayed from dispersion, and broadened from scattering during the eclipse egress.

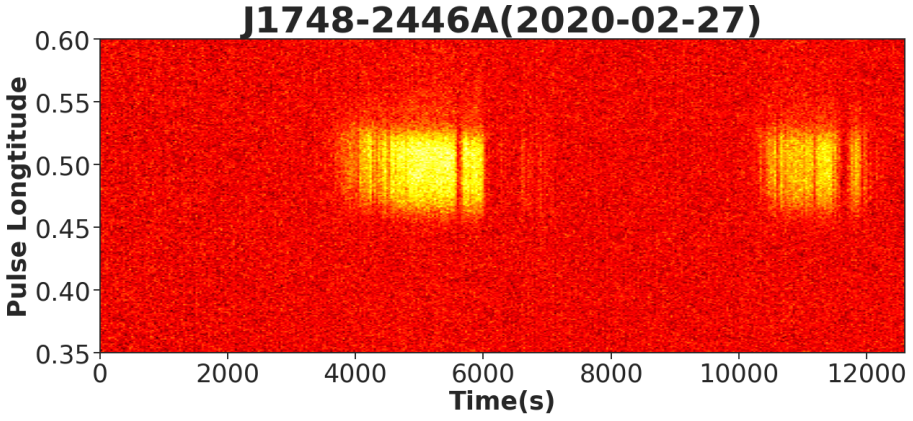

Figure 3.3: Observation 2 data showing pulse longitude over 12593 s ($\sim$ 2 orbits) of the PSR J1748−2446A binary. We have zoomed in on the pulse longitude and observe the pulse being delayed from dispersion, and broadened from scattering during the eclipse egress.

Chapter 4

Methods

4.1 Software

4.1.1 Pre-processing

As described in Section 3.3 we recorded search mode data of the Globular Cluster, Terzan 5, with the MeerKAT beam centered on PSRs J1748−2446N and J1748−2446O. These high time resolution filterbank files, that have three data dimensions namely time, frequency and polarisation state, were folded into PSR J1748−2446A pulsar archive files using `dspsr`[1] and an up-to-date folding ephemerides. The resulting files had data resolutions as given in Table 3.1 and are formatted such that they can be analysed using a standard pulsar software, called PSRCHIVE, as described next.

4.1.2 PSRCHIVE

We made use of `PSRCHIVE`[2] and its adaptable set of sub-routines for data analysis and processing. PSRCHIVE is an open source collection of software libraries and utilities for working with pulsar astronomical data. It meets the challenges posed by different data formats and processing requirements encountered in pulsar observations (Hotan et al., 2004). It is designed for handling high time resolution data from radio telescopes, allowing for calibration, RFI mitigation, data visualization, and various analysis tasks. Radio frequency interference (RFI) refers to the unwanted or non-astrophysical signals that can interfere with the genuine astrophysical signals being observed by radio telescopes (Taylor and Hulburt, 1926). We made use of

[1] https://dspsr.sourceforge.net/
[2] https://psrchive.sourceforge.net/

both command-line processing and Jupyter notebook-based analysis as PSRCHIVE supports interactions through Python.

4.1.3 DMfitter

This is code by Lin et al. (2021), `dmfitter`[3], that provides a toolkit for analyzing changes leading to a frequency-dependent delay in arrival times and a broadening of the pulses, allowing the user to make use of precise measurement of the dispersion measure and pulse scattering. The code performs template matching in the Fourier domain, following the framework of Pennucci et al. (2014), to fit the DM, thus enabling the correction of dispersion effects as described in Section 2.1. It also fits for scattering effects by implementing the previously described exponential decay function, and its frequency dependence as described in Equation 2.5 within the Fourier domain. We made use of these tools to measure changes in DM and scattering.

4.2 Data analysis

4.2.1 RFI cleaning

As defined in the above section, RFI is unwanted or non-astrophysical signals and these RFI signals can come from satellites and terrestrial sources, such as man-made sources from electronics. Even though MeerKAT is located in a remote RFI quiet environment we still see RFI in our data, especially due to overhead satellites. Our data had RFI which we removed using PSRCHIVE tools to clean it. We zero-weighted frequency channels that were affected by RFI by manually masking these specific channels to be ignored from the subsequent analysis, as shown in Figure 4.1.

4.2.2 Data reduction

With the usage of PSRCHIVE we reduced the frequency resolution of our data by averaging over frequency channels by the process called frequency scrunching. We frequency scrunched Observation 1 and Observation 2 to 16 channels only for measuring DM and scattering variations. We have also reduced the number of subintegrations, for Observation 1 to 300 and Observation 2 to 388, by averaging our data over multiple integrations (time bins) through time scrunching. These reductions simplified data visualization and analysis and they improved the "signal-to-noise" ratio (SNR) making it easier to detect the pulse shape from the pulsar. This made profile fitting faster and since our SNR has increased we could see the pulse per subintergration more clearly.

[3]https://github.com/quantumfx/dmfitter

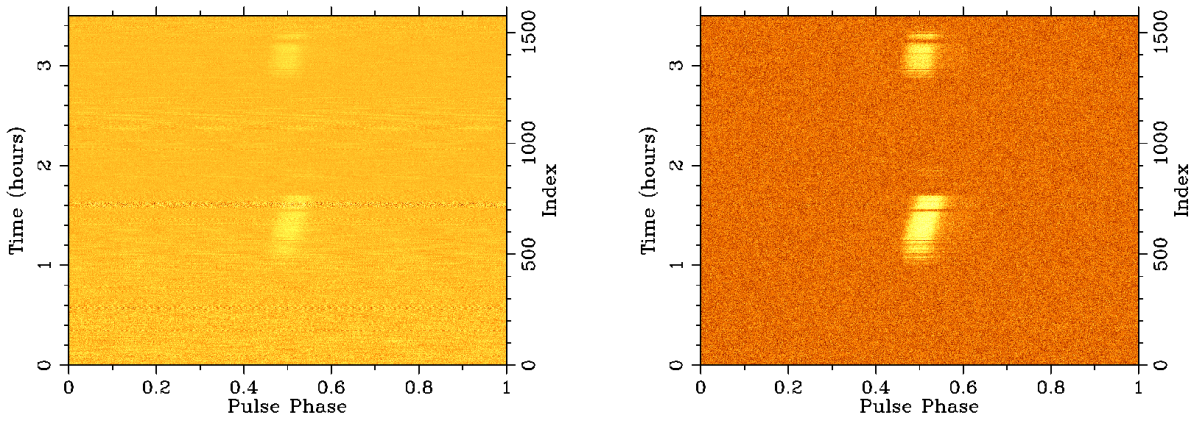

Figure 4.1: Comparison of our Observation 2 data showing the effect of RFI cleaning. Left: The raw, unclean data, with interference present. Right: Our data after RFI mitigation, displaying enhanced signal clarity.

As described in Section 2.3 different frequencies from the same pulse arrive at the telescope at slightly different times and this delay in arrival times spreads out or "smears" the original sharp pulse, making it harder to analyze. We corrected for this smearing by a process called dedispersion which aims to realign the signals from all frequencies so that they all effectively arrive at the same time, reconstructing the original sharp pulse.

We also subtracted the off-pulse baseline, to rescale the data such that it has a baseline centered on zero (Figure 4.2).

4.2.3 Improving ephemerides

Ephmerides are the collections of parameters written in a table format that provide the position of our pulsar at given times. Due to the unique environment of spider binaries our epoch of periastron described in Section 3.3, T0, changes between epochs (or over time). This change may be a result of mass transfer and accretion, strong gravitational attraction or changes in the companion star itself among various reasons.

We adjusted our Observation 1 T0 to 58500.4861165 MJD, approximately a 0.665 s correction, in order to straighten or align the pulse emission in phase across the full observation. We similarly adjusted our Observation 2 T0 to 58500.4861 MJD, approximately a 2.09 s correction. Our pulse profiles were still not correctly aligned

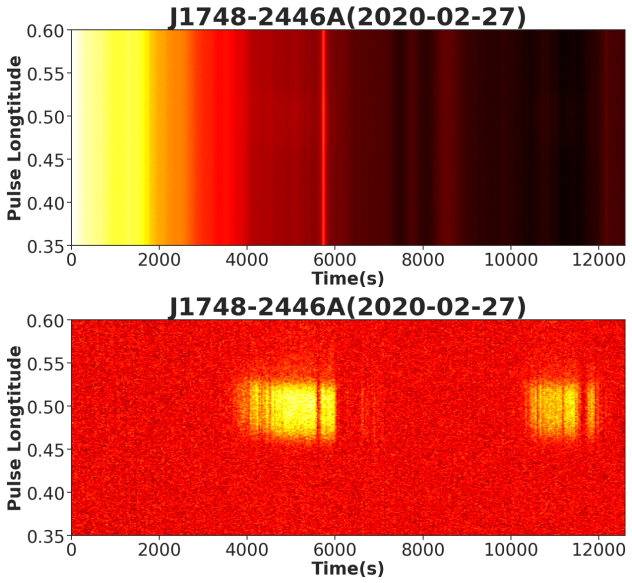

Figure 4.2: Comparison of our Observation 2 data showing the effect of removing the off-pulse baseline. Top: Before removing baseline. Bottom: Our data after removing the baseline.

in phase across observing time so we searched for DM using a sub-routine in psrchive called `pdmp` and installed a new DM of 242.4527, as shown in Figure 4.3.

4.2.4 Polarisation calibration

In this thesis we will be using both the total intensity pulsar data (Stokes I), as well as the polarization vectors (Stokes Q, U, V) to investigate the pulsar's polarization properties and to measure changes in the RM as described in Section 2.2. We therefore have to ensure that the data is polarisation calibrated for these purposes.

Since our data predates the automatic polarisation calibration of MeerKAT pulsar data, we had to apply the polarisation calibration solutions manually using a sub-routine within `PSRCHIVE` called `pac`, together with calibration solutions obtained from MeerKAT.

As part of the array preparation observations ahead of our observations on PSR J1748−2446A, the telescope visits a calibrator with well-known polarisation properties, such as PSR J0408−6545 or PSR J1939−6342. These observations are then used to obtain calibration solutions in the form of a Jones matrix, as described in detail in Serylak et al. (2021), which gets stored in a configuration file.

Applying these configuration files to our data, ensures that all delays and phase

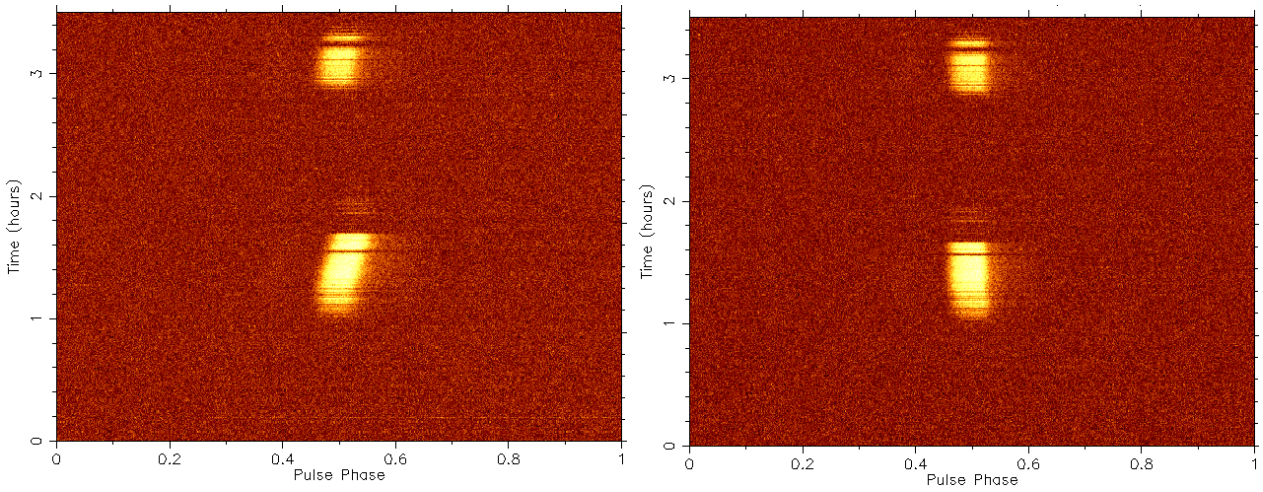

Figure 4.3: Comparison of our Observation 2 profiles. Left: profile with the original data. Right: profile after installing a new T0 and DM

offsets between the two polarisation streams (horizontal and vertical) as recorded by the MeerKAT L-band receiver have been corrected. Additional information regarding MeerKAT polarisation calibration can also be found online on their user documentation pages [4].

4.2.5 Measuring DM and change in DM

In order to measure changes in DM across the orbit of the binary, we choose time samples away from the eclipse that appear unaffected by the companion wind to create a template to compare other phases of the pulsar orbit to. We used this template to smooth our data to reduce noise.

To help us decide which subintegrations contained real detections of the pulse shape, in the dynamic eclipsing spider binary environment, we compared all subintegrations to the brightest subintegration and computed how similar their shapes are using a similarity function. To achieve this we used the Cosine similarity function as implemented in `sklearn`. This involved sampling our pulse shape at regular subintegrations to create a vector representation of the pulse. The cosine similarity between these vector representations of the pulse shapes are thereafter computed, with a high percentage value indicating a high degree of similarity. In reviewing the output, we find that keeping the subintegrations with a similarity index of 60% or higher all contain pulse detections. Thereafter we computed the dispersion measure on the obtained trusted subintegrations above, using the `dmfitter` code described in the

[4]https://skaafrica.atlassian.net/wiki/spaces/ESDKB

previous section, to infer whether we see changes in DM or not.

4.2.6 Measuring RM and change in RM

The initial rotation measure value was incorrectly set to zero in the meta data of our observations, so our first task was to reset the RM to the known value for Terzan 5A of $180\,\mathrm{rad\,m^{-2}}$. This adjustment was essential for us to be able to measure potential additional Faraday rotation effects, and therefore changes in RM.

Previous studies carried out by You et al. (2018) and Li et al. (2023) have investigated changes in rotation measure for Terzan 5A. You et al. (2018) the Parkes 64m radio telescope to conduct analysis of frequency-dependent characteristics over different frequency bands (728 MHz, 1369 MHz, and 3100 MHz). In contrast, Li et al. (2023) took use of the 100m Green Bank Telescope's capabilities, focusing on higher frequency bands around 1.5 GHz and 2 GHz.

In light of RM variations up to $25\,\mathrm{rad\,m^{-2}}$ for every 3 minutes of observing time by You et al. (2018) and variations of up to $100\,\mathrm{rad\,m^{-2}}$ for every 20 seconds by Li et al. (2023), we segmented the data into single subintegrations. Evaluating RM changes on shorter timescales helps us detect rapid changes, especially when the pulsar signal undergoes periodic eclipses when passing behind its companion star. We used `PSRCHIVE (rmfit)` to search for the rotation measure value of each sub integration.

After obtaining the best RM values per subintegration as produced by `rmfit`, we checked the validity of these measurements using the following steps. We first make the general cut of only considering subintegrations for which the Stokes I SNR is larger than 15. The SNR values were obtained using `psrstat` within `PSRCHIVE`. We then calculated the linearly polarised intensity, L, using the formula $L = \sqrt{Q^2 + U^2}$ (Lorimer and Kramer, 2004), for each subintegration. Then we checked if there was any improvement in the SNR of the linearly polarised signal, compared to the SNR before we applied a new RM value. If the increase in SNR was higher by a factor of 20%, we concluded that the applied RM value was indeed a real measurement. Where we saw no increase in the linear SNR after applying a new RM value, we disregarded that RM fit value. This was done since the `rmfit` software will always find a best-fit value. Our checks were therefore necessary to ensure the RM values returned by `rmfit` were indeed physical.

We note that `rmfit` returns RM measurements with defined error bars for only a small set of analysed subintegrations. The software was not able to constrain the errors for the majority of the RM values returned. For this reason we will use the standard deviation of the RM values away from eclipse as a conservative error

estimate.

Chapter 5

Results

In this chapter we describe the changes in DM, scattering and RM, as obtained using the methods in Chapter 4. We also discuss their implications for our study.

5.1 Reference template

All changes in DM (ΔDM) and changes in scattering ($\Delta\tau$) described in this chapter are measured relative to a template. To construct a template we have picked subintegrations that are distant from the eclipse as our template so we are able to measure variations in DM and scattering. This ensures that our template is not affected by plasma from the companions outflow. The changes ΔDM and $\Delta\tau$ in this chapter are measured relative to template values, where $\Delta value$ = subint value - template value.

We therefore mainly expect positive ΔDM and $\Delta\tau$ values, since the DM and τ of the template represents only ISM plasma dominated values. Sometimes we can get smaller values compared to the template (i.e. negative ΔDMs or $\Delta\tau$s), but these are often associated with larger error bars, and are expected to come from uncertainties associated with the covariance of DM and scattering.

Our template profile is of course brighter than an averaged profile across all data, because in the averaged profile we have added all the subintegrations including eclipsed subintegrations (where there are non-detections). This inclusion of additional noise lowers the SNR of the averaged profile as observed in Figure 5.1. Our Observation 1 template is about 1.75 times that of its averaged profile, whereas in Observation 2 it is about 3 times the averaged profile.

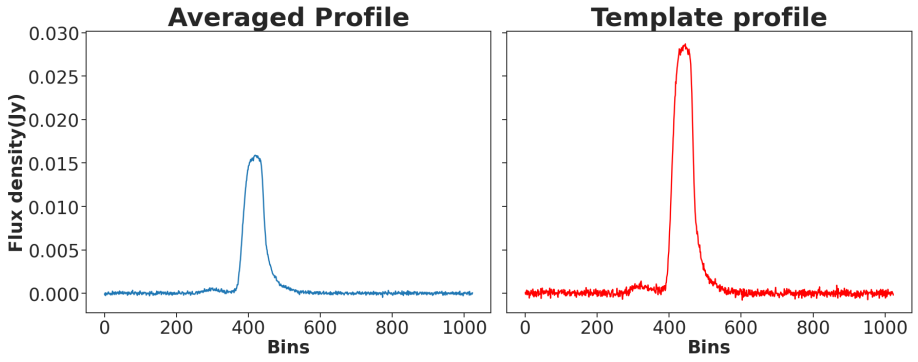

Figure 5.1: Observation 1 profile comparisons. Left: The averaged emission profile across the full observing duration (i.e. including eclipses). Right: The pulsar's emission profile observed far from the eclipse (between 4000 s and 6500 s), unaffected by the companion star's material.

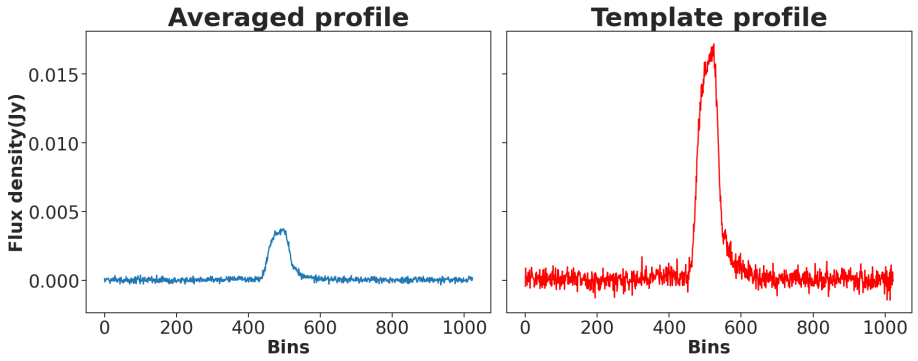

Figure 5.2: Observation 2 profile comparisons. Left: The averaged emission profile across the full observing duration (i.e. including eclipses). Right: The pulsar's emission profile observed far from the eclipse (between 5000 s and 6500 s), unaffected by the companion star's material.

5.2 DM variations

In Observation 1 we recorded a DM change, ΔDM, with a maximum of $0.077\,\mathrm{pc\,cm^{-3}}$ during the eclipse ingress around 1400 s. During the egress starting at around 2400 s we recorded an increase to a maximum of $\Delta DM = 0.089\,\mathrm{pc\,cm^{-3}}$, as shown in Figure 5.3.

In Observation 2, during the first eclipse egress we see a decrease in DM from a maximum of $\Delta DM = 0.055\,\mathrm{pc\,cm^{-3}}$ during the eclipse ingress. We also record some DM variations of $\Delta DM = 0.028\,\mathrm{pc\,cm^{-3}}$during the eclipse just after 6000 s. In the second eclipse egress we observe a maximum change of $\Delta DM = 0.032\,\mathrm{pc\,cm^{-3}}$, as

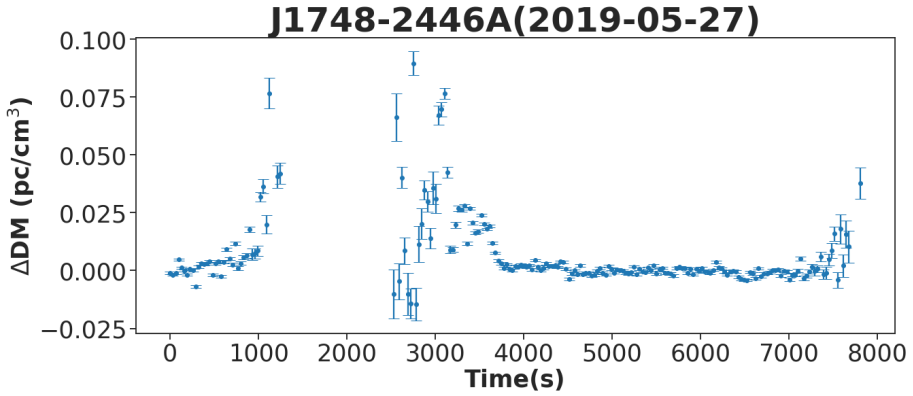

Figure 5.3: Observation 1 DM variation over time. During the eclipse ingress we see an increase in DM and during the egress we observe an unusual pattern where there is an increase followed by a decrease in DM.

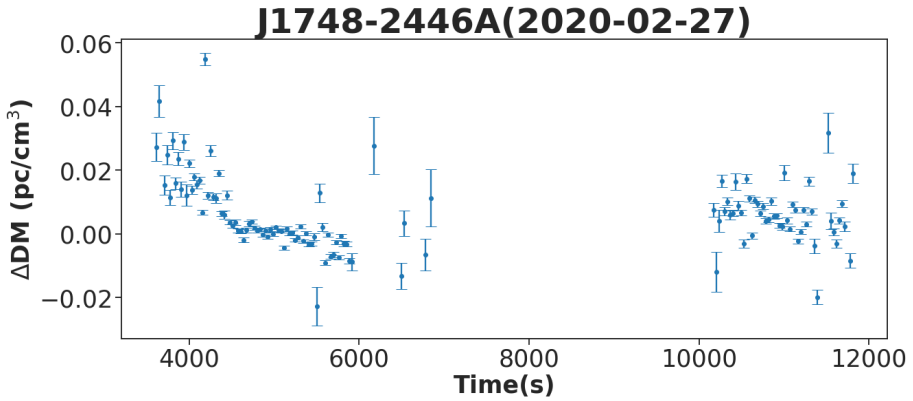

Figure 5.4: Observation 2 DM variation over time. During the first eclipse egress we see an decrease in DM followed by DM values with large error bars when the signal becomes faint.

shown in Figure 5.4.

Both of our observation recordings are consistent with the $0.1\,\mathrm{pc\,cm^{-3}}$ variations from You et al. (2018), which validates the observational the methods and analytical approaches applied in my study.

The fastest DM change rate we observe in Observation 1 is $0.0011\,\mathrm{pc\,cm^{-3}\,s^{-1}}$, between 3104 seconds and 3168 seconds with a ΔDM difference of $0.067\,\mathrm{pc\,cm^{-3}}$. In Observation 2 the fastest change rate is $0.0015\,\mathrm{pc\,cm^{-3}\,s^{-1}}$, between 4160 seconds and 4192 seconds with a ΔDM difference of $0.048\,\mathrm{pc\,cm^{-3}}$.

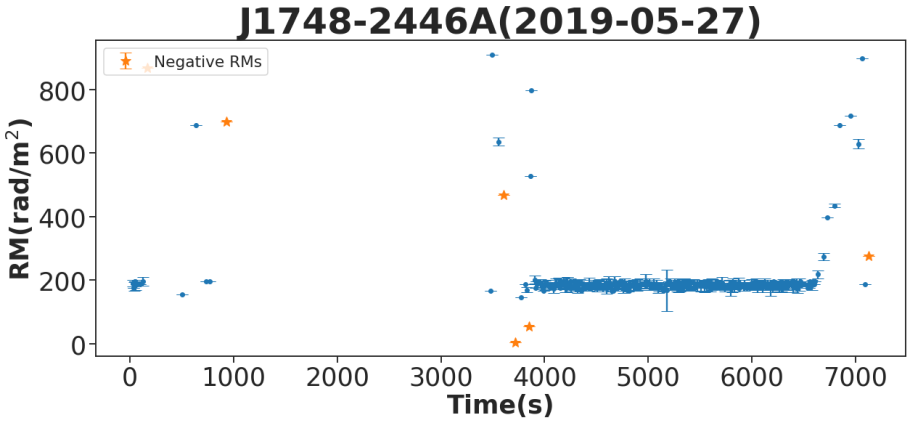

Figure 5.5: Observation 1 RM variations over time. We see extreme fluctuations during the eclipse ingress and egress. Note: Negative RM values (orange points) have been plotted as their absolute value for ease of visualisation.

5.3 RM variations

As expressed in Section 4.2.6 we use the standard deviation of the spread of RM values obtained away from eclipse to estimate an uncertainty of our RM values. In Observation 1 between 4000 s and 6500 s we find a standard deviation of 8.73 rad m^{-2}, and in Observation 2 between 5000 s and 6000 s a standard deviation of 4.1 rad m^{-2}. We use the rounded maximum value these two estimates, i.e. $\sim$10 rad m^{-2}, as the uncertainty on all RM values in this section.

In Observation 1 we observed an unusual range of RM fluctuations, with variations measuring a great change of -869 rad m^{-2} during the ingress and a maximum change of 910 rad m^{-2} in the egress phase, see Figure 5.5. This is a big contrast to the more moderate fluctuations reported in other studies such as the +/-5 rad m^{-2} fluctuations observed by You et al. (2018) since we were looking at shorter timescales as mentioned in the previous section.

In Observation 2 recorded a minimum of -748 rad m^{-2} during the first eclipse egress. We recorded a few rapid fluctuations during the second egress recording an RM maximum of 769 rad m^{-2} and a minimum of -337 rad m^{-2}, see Figure 5.6.

Most notably, these RM fluctuations correlated positively with improvements in the linear polarization of the signal, see for example Figure 5.7, providing confidence in our results.

The fastest RM change rate we observe in Observation 1 is 22 rad m^{-2} s^{-1}, between 7064 seconds and 7096 seconds with a ΔRM difference of 714 rad m^{-2}. In Obser-

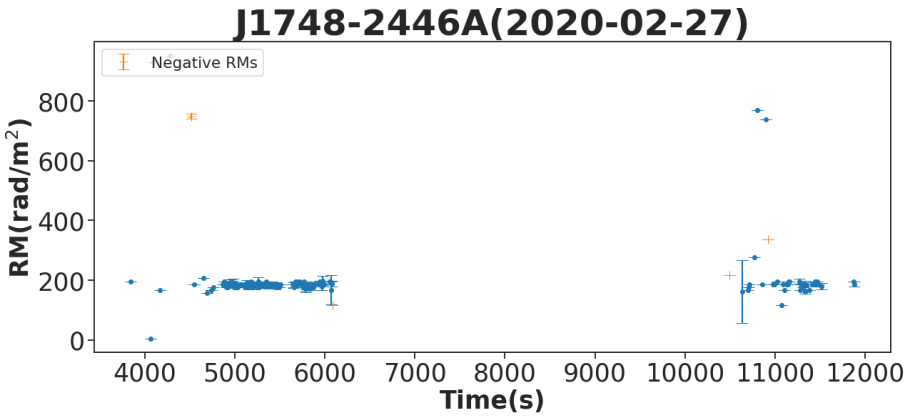

Figure 5.6: Observation 2 RM variations over time. We see extreme fluctuations during the eclipse ingress. Note: Negative RM values (orange points) have been plotted as their absolute value for ease of visualisation.

vation 2 the fastest change rate is $7\,\mathrm{rad\,m^{-2}\ s^{-1}}$, between 4168 seconds and 4280 seconds with a ΔRM difference of $784\,\mathrm{rad\,m^{-2}}$.

The measured rate of over $20\,\mathrm{rad\,m^{-2}\ s^{-1}}$, show that with the sensitivity of the MeerKAT data we observe changes in RM that are at least four times more rapid than those reported in You et al. (2018) and Li et al. (2023) which we compute from their work as $0.14\,\mathrm{rad\,m^{-2}\ s^{-1}}$ and $5\,\mathrm{rad\,m^{-2}\ s^{-1}}$ respectively.

5.4 Scattering

Our measured scattering variations are reflected in the observed changes in exponential scattering tails, typical of multi-path propagation of an inhomogenous medium. The profile shape changes as the pulsar transitions through an eclipse are shown in Figure 5.8.

In Observation 1 we recorded a change in scattering of up to a maximum of 661.41 μs, see Figure 5.9. For Observation 2 we recorded smaller variations in scattering of up to a maximum of 36.17 μs, see Figure 5.10. These are the first records of scattering changes measured for PSR J1748−2446A.

5.5 DM, RM and scattering relation

DM, RM and scattering are all closely related as they all describe how plasma impacts our pulsars signal. Like we mentioned above DM is a measurement of the

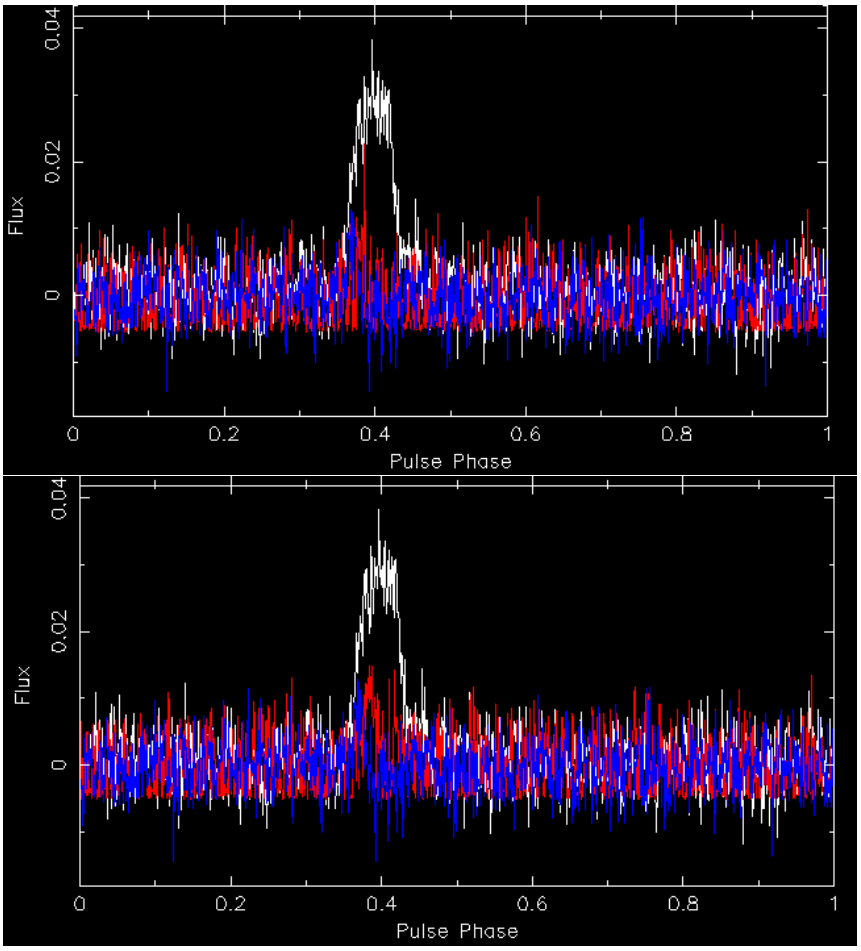

Figure 5.7: Comparison of a single subintegration linear polarisation of our Observation 1 data. We see an improvement in the linear (red line) after installing the new RM value. Top: Old RM value, for which the Stokes L SNR value is 8.09. Bottom: After installing the new RM value we obtain a Stokes L SNR value of 13.26.

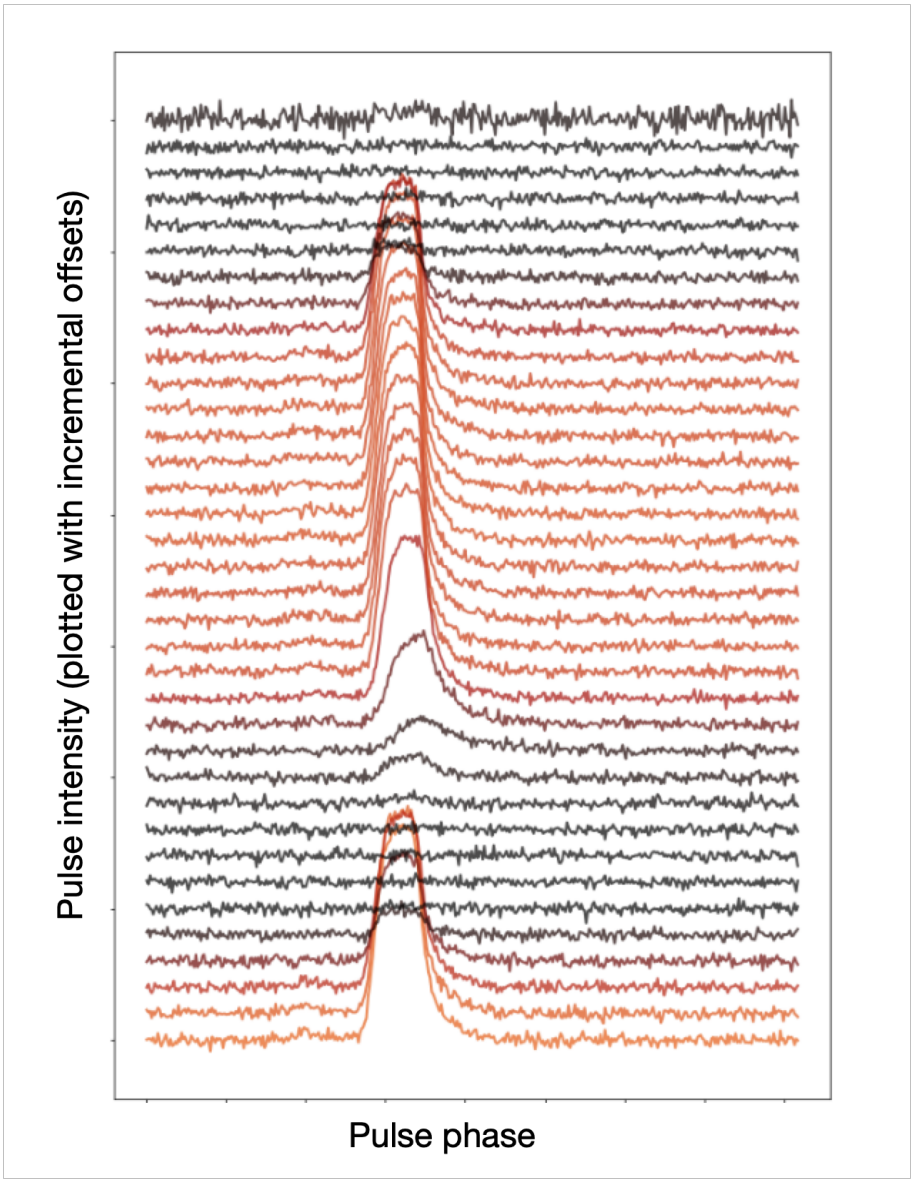

Figure 5.8: The pulse profiles associated with time samples close to the eclipse for Observation 1 are plotted sequentially, along the y-axis, and with each pulse plotted with an arbitrary intensity offset to make them visible. Pulses close to the eclipse clearly exhibit an exponential scattering tail which broadens deeper into the eclipse. The plotted colors scales linearly with the maximum amplitude value of each pulse and subintegrations have been averaged together for further improved visualization of the sequence.

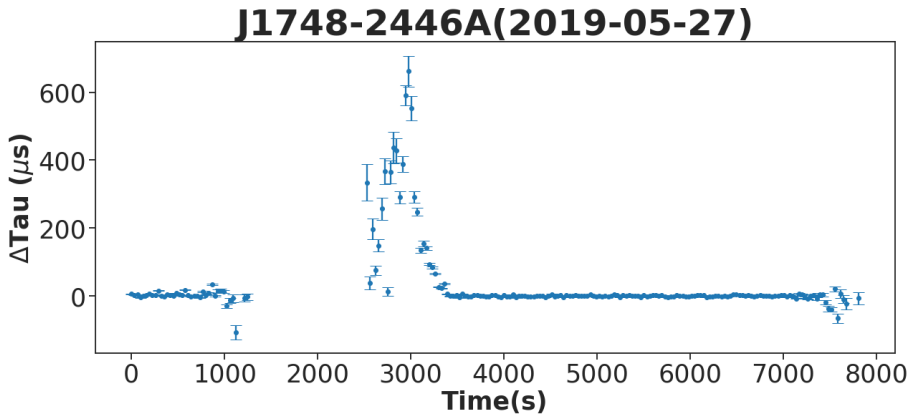

Figure 5.9: Observation 1 scattering variation over time. We see no changes during the eclipse ingress but real measurable changes during the exit. During the egress we observe an increase followed by a decrease which is consistent with the pulse broadening.

total number of free electrons along the line of sight and this directly impacts the time delay of the signal while RM is observed in changes in the polarisation plane of the emission.

In our study we observe DM, RM and scattering simultaneously being affected by the companions outflow.

In Observation 1 we observe that ΔDM is positively correlated to $\Delta\tau$ as can be seen in Figure 5.11. The same changes we observe in ΔDM in time we also observe in $\Delta\tau$. Even though we measure extreme RM variations in the ingress and egress we cannot measure some RM values closer to the eclipse, where we expect extreme Faraday rotation because the magnetic fields strength is intense. Furthermore RM changes are likely happening on faster timescales close to the eclipse and since our data's time resolution is 8 s we can not measure the RM variations because it is changing too fast.

The positive correlation among ΔDM, ΔRM, and $\Delta\tau$ indicate that our companions outflow has a combination of high electron densities, strong magnetic fields, and significant electron density inhomogeneities.

5.6 Magnetic field

Since we have measured ΔDM and ΔRM we are able to estimate the magnetic field strength of our companions material. The magnetic field strength can be obtained

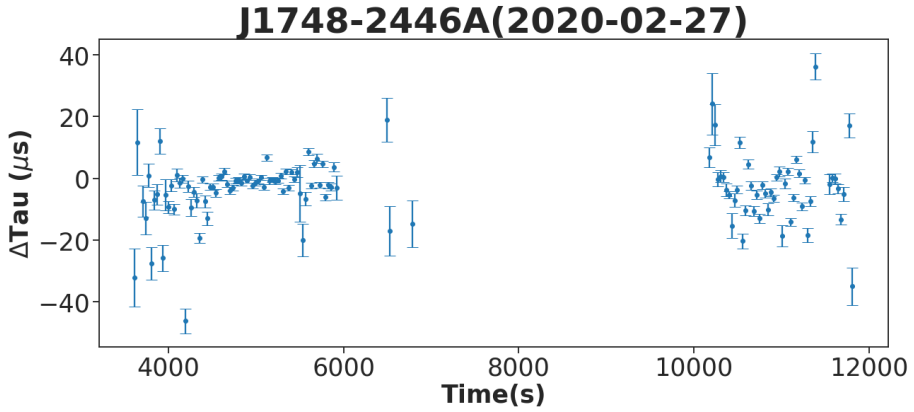

Figure 5.10: Observation 2 scattering variation over time. We observe small scattering changes during the eclipse ingress/egress.

from

$$B_{\parallel} = 1.232 \frac{\Delta RM}{\Delta DM}, \tag{5.1}$$

where $B_{\parallel}$ is in microGauss (μG) assuming that the changes in DM and RM are dominated by the same magneto-ionic plasma.

We picked a ΔRM value and its corresponding ΔDM value and using an error estimate of 10 rad m^{-2} in RM and 0.001 pc cm^{-3} in DM, we were able to compute the companions material's magnetic field strength.

In Observation 1 the largest negative RM value that had a corresponding measured ΔDM(0.018 pc cm^{-3}) is -467 rad m^{-2}. The change in RM (ΔRM) is computed by ΔRM = RM - 180 rad m^{-2}, which is -647 rad m^{-2} in this case. We were able to compute the companions material's magnetic field strength and found -43 ± 2 milliGauss (mG). Similarly, when RM was at its positive maximum of 910 rad m^{-2}, $\Delta RM = 730$ rad m^{-2}, with the corresponding ΔDM of 0.017 pc cm^{-3} we calculated a magnetic field's strength of 57 ± 4 mG.

In Observation 2 the largest negative RM value that had a corresponding measured ΔDM(0.019 pc cm^{-3}) is -881 rad m^{-2}, ΔRM = -1061 rad m^{-2}. We were able to compute the companions material's magnetic field's strength of -66 ± 3 mG. When RM was at its maximum of 950 rad m^{-2}, $\Delta RM = 770$ rad m^{-2}, with the corresponding ΔDM of 0.026 pc cm^{-3} we calculated a magnetic field's strength of 38 ± 2 mG.

These values are an order of magnitude larger than the Crab nebula's magnetic field strength which is estimated to be about 10^{-3} Gauss (G) (George et al., 1999).

Since we cannot measure some RM values in the eclipse ingress and egress we can

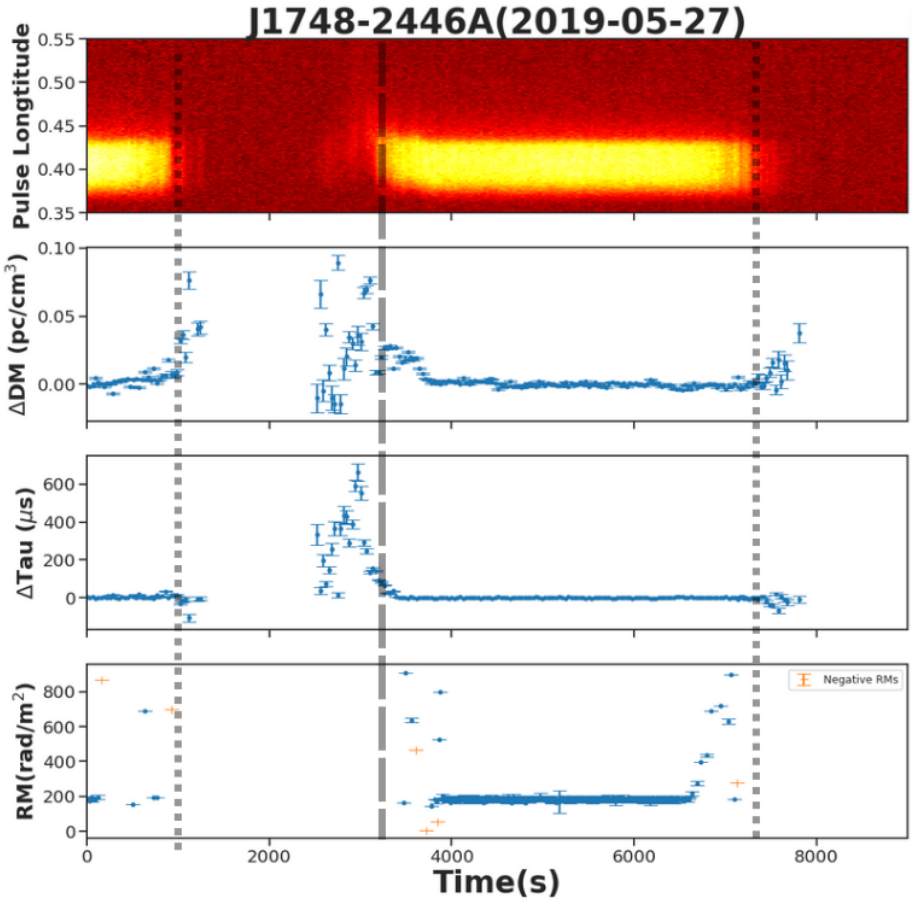

Figure 5.11: Observation 1's ΔDM, RM and $\Delta\tau$'s comparisons across time. We observe an increasing trend in the eclipse ingress (dotted lines) and egress (dashed line) where higher electron densities, stronger magnetic fields, and inhomogeneities exist.

estimate them given the magnetic field strength and ΔDM. When ΔDM is at its maximum, $0.089\,\mathrm{pc\,cm^{-3}}$, we can estimate the RM to be approximately $4100\,\mathrm{rad\,m^{-2}}$ assuming the magnetic field strength is 57 mG. This value is consistent with the study in Li et al. (2023). The authors estimate extreme variations in RM, often exceeding $3000\,\mathrm{rad\,m^{-2}}$ at the eclipse egress and ingress.

5.7 Changes in circular polarisation

When radio waves travel through magneto-ionic plasma, the plasma can convert linear polarisation into circular polarisation (Stokes V) and circular to linear polari-

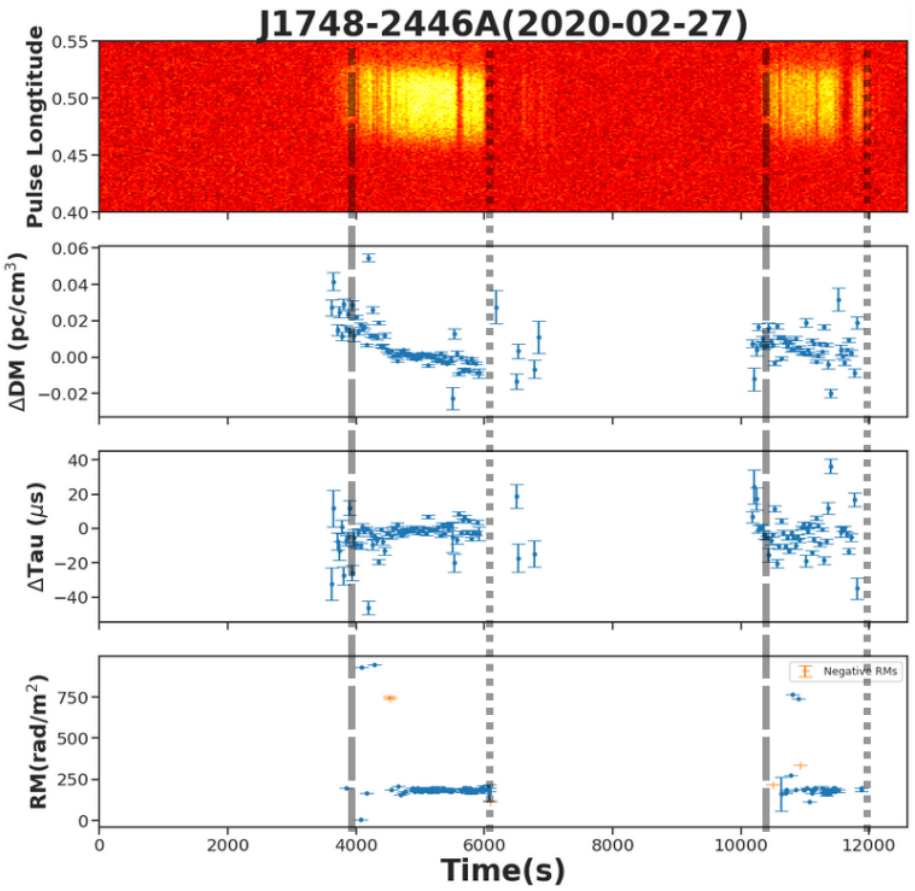

Figure 5.12: Observation 2's ΔDM, RM and $\Delta\tau$'s comparisons across time. While not as prominent as in Observation 1's data, we do observe changes in these quantities during the eclipse ingress (dotted lines) and egress (dashed lines) where higher electron densities, stronger magnetic fields, and inhomogeneities exist.

sation (Vedantham and Ravi, 2019). We looked for changes in Stokes V at MeerKAT L-band, in the brightest observing epoch (Observation 1), but found none. It has been seen at higher frequencies (Li et al., 2023) deeper into the eclipse (or closer to the companion's surface). Faraday conversion is expected in only very strong magnetic fields environments, implying that magnetic fields are stronger than what we measured closer to companion surface. Based on their observations Li et al. (2023) estimated a magnetic field near superior conjunction through their Faraday conversion estimates of > 10 Gauss (G).

5.8 Plasma lensing

We briefly worked with Simon Ho from Swinburne University, and a member of the Meertime research group. By providing him with the exact timestamps associated with ingress and egress for Observation 1, he was able to find approximately ten single pulses close to eclipse with SNR > 10. Such an SNR value is much brighter than the average SNR per pulse rotation, which we calculated the brightest to be 1-2 SNR, indicating that they are likely magnified single pulse worth further investigation.

These are consistent with the study on Terzan 5A by Bilous et al. (2019), where they observed unusually bright single pulses (BSPs) near eclipse ingress and egress. They observed BSPs magnified by factors of up to 40 times the averaged pulse flux. Because the BSPs observed are similar to those from another binary pulsar, B1957+20, which were considered to be caused by companions outflow, (Main et al., 2018), they argue that strong lensing likely occurs in Terzan 5A as well.

While these bright single pulses we found are clearly boosted in SNR, an SNR of 10 and finding only ten pulses, is not a large or bright enough sample of single pulses to warrant an in-depth analysis of RM, DM and scattering measurements of these single pulses. Ideally we would want to find single pulses that are 50 - 100 times brighter for detailed analysis of single pulse behaviour. Finding such exceptionally brightly lensed pulses in Terzan 5A would allow us to instantaneously measure the RM and the magnetic field strength further into the eclipse.

Chapter 6

Conclusion

6.1 Conclusions

In this work we have analysed two observations of the spider binary pulsar PSR J1748−2446A using MeerKAT L-band data, to characterise its eclipsing properties. Across two observing epochs we measure changes in DM, RM and scattering and quantify them carefully.

We record a maximum DM change of $0.09\,\mathrm{pc\,cm^{-3}}$ in Observation 1 and of $0.055\,\mathrm{pc\,cm^{-3}}$ in Observation 2 which are both consistent with the $0.1\,\mathrm{pc\,cm^{-3}}$ variations from You et al. (2018). This means that there are variations in the electron density along the line of sight, due to dynamic changes in the companion's outflow.

We measured scattering changes and this is the first time these changes have been measured for PSR J1748-2446A. We measured a maximum change of $661.41\,\mu$s and a minimum of $0.018\,\mu$s for Observation 1. For Observation 2 we measured a maximum change of $36.17\,\mu$s and a minimum of $0.11\,\mu$s. The companion outflow has irregularities and inhomogeneities, it is dynamic as we measure up to 8 times our pulse period.

We measured extreme RM variation of +/-900 $\mathrm{rad\,m^{-2}}$ during the ingress and egress phases for both Observation 1 and Observation 2, these are a big contrast to the +/-5 $\mathrm{rad\,m^{-2}}$ variations observed by You et al. (2018). We also measure a maximum rate of change in RM of over $20\,\mathrm{rad\,m^{-2}\,s^{-1}}$, significantly higher than previously observed. These extreme change suggests that the companion's outflow is highly magnetized.

Given these changes in RM and DM we were able to estimate the companions outflow magnetic field strength to be $57 \pm 4\,\mathrm{mG}$.

6.2 Future work

We would like to investigate the rate of RM changes on shorter time scales than investigated in this work, where we used 8 s subintegrations, by using single pulses, which means we can study changes on the timescale of the pulse period, 11.56 ms.

Single pulses are weak and can be hidden in the noise hence this can only be done for bright single pulses such as pulses which are magnified through plasma lensing. We would like to investigate the RM and DM changes of such bright single pulses. A further improvement in SNR values of single pulses, for continued studying, could come from MeerKAT data where we specifically centre the MeerKAT beam on Terzan 5A. Longer duration observations, or multiple epochs, will improve our chances of detecting brightly plasma lensed pulses.

We also would like to look at the MeerKAT S-band, which is now scientifically operational and centered at higher frequencies (1750 MHz - 3500 MHz), to study the magnetic fields and to investigate the polarisation properties of Terzan 5A. At higher frequencies, radio waves are less impacted by the plasma's propagation effects described in this work, allowing us to observe more deeply into the companion star outflow. In particular we would like to study the circular polarisation of Terzan 5A, to see if we observe Faraday conversion as described in Section 5.7, which will give additional insight into the extreme magnetic environment of the companion star. Understanding these phenomena in spider binaries could ultimately lead us to understanding the emission processes in some FRBs where similar processes have been observed (Xu et al., 2022; Luo et al., 2020).

Bibliography

M. A. Alpar, A. F. Cheng, M. A. Ruderman, and J. Shaham. A new class of radio pulsars. , 300(5894):728–730, Dec. 1982. doi: 10.1038/300728a0.

M. Bailes, E. Barr, N. D. R. Bhat, J. Brink, S. Buchner, M. Burgay, F. Camilo, D. Champion, J. Hessels, A. Jameson, S. Johnston, A. Karastergiou, R. Karuppusamy, V. Kaspi, M. Keith, M. Kramer, M. McLaughlin, K. Moodley, S. Oslowski, A. Possenti, S. Ransom, F. Rasio, J. Sievers, M. Serylak, B. Stappers, I. Stairs, G. Theureau, W. van Straten, P. Weltevrede, and N. Wex. MeerTime - the MeerKAT Key Science Program on Pulsar Timing. In *MeerKAT Science: On the Pathway to the SKA*, page 11, Jan. 2016. doi: 10.22323/1.277.0011.

M. Bailes, A. Jameson, F. Abbate, E. D. Barr, N. D. R. Bhat, L. Bondonneau, M. Burgay, S. J. Buchner, F. Camilo, D. J. Champion, I. Cognard, P. B. Demorest, P. C. C. Freire, T. Gautam, M. Geyer, J. M. Griessmeier, L. Guillemot, H. Hu, F. Jankowski, S. Johnston, A. Karastergiou, R. Karuppusamy, D. Kaur, M. J. Keith, M. Kramer, J. van Leeuwen, M. E. Lower, Y. Maan, M. A. McLaughlin, B. W. Meyers, S. Osłowski, L. S. Oswald, A. Parthasarathy, T. Pennucci, B. Posselt, A. Possenti, S. M. Ransom, D. J. Reardon, A. Ridolfi, C. T. G. Schollar, M. Serylak, G. Shaifullah, M. Shamohammadi, R. M. Shannon, C. Sobey, X. Song, R. Spiewak, I. H. Stairs, B. W. Stappers, W. van Straten, A. Szary, G. Theureau, V. Venkatraman Krishnan, P. Weltevrede, N. Wex, T. D. Abbott, G. B. Adams, J. P. Burger, R. R. G. Gamatham, M. Gouws, D. M. Horn, B. Hugo, A. F. Joubert, J. R. Manley, K. McAlpine, S. S. Passmoor, A. Peens-Hough, Z. R. Ramudzuli, A. Rust, S. Salie, L. C. Schwardt, R. Siebrits, G. Van Tonder, V. Van Tonder, and M. G. Welz. The MeerKAT telescope as a pulsar facility: System verification and early science results from MeerTime. , 37:e028, July 2020. doi: 10.1017/pasa.2020.19.

A. V. Bilous, S. M. Ransom, and P. Demorest. Unusually bright single pulses from the binary pulsar b1744–24a: A case of strong lensing? *The Astrophysical Journal*, 877(2):125, jun 2019. doi: 10.3847/1538-4357/ab16dd. URL `https://dx.doi.org/10.3847/1538-4357/ab16dd`.

R. Buschauer and G. Benford. General theory of coherent curvature radiation. , 177:109–136, Oct. 1976. doi: 10.1093/mnras/177.1.109.

F. Camilo, P. Scholz, M. Serylak, S. Buchner, M. Merryfield, V. M. Kaspi, R. F. Archibald, M. Bailes, A. Jameson, W. van Straten, J. Sarkissian, J. E. Reynolds, S. Johnston, G. Hobbs, T. D. Abbott, R. M. Adam, G. B. Adams, T. Alberts, R. Andreas, K. M. B. Asad, D. E. Baker, T. Baloyi, E. F. Bauermeister, T. Baxana, T. G. H. Bennett, G. Bernardi, D. Booisen, R. S. Booth, D. H. Botha, L. Boyana, L. R. S. Brederode, J. P. Burger, T. Cheetham, J. Conradie, J. P. Conradie, D. B. Davidson, G. De Bruin, B. de Swardt, C. de Villiers, D. I. L. de Villiers, M. S. de Villiers, W. de Villiers, C. De Waal, M. A. Dikgale, G. du Toit, L. J. du Toit, S. W. P. Esterhuyse, B. Fanaroff, S. Fataar, A. R. Foley, G. Foster, D. Fourie, R. Gamatham, T. Gatsi, R. Geschke, S. Goedhart, T. L. Grobler, S. C. Gumede, M. J. Hlakola, A. Hokwana, D. H. Hoorn, D. Horn, J. Horrell, B. Hugo, A. Isaacson, O. Jacobs, J. P. Jansen van Rensburg, J. L. Jonas, B. Jordaan, A. Joubert, F. Joubert, G. I. G. Józsa, R. Julie, C. C. Julius, F. Kapp, A. Karastergiou, F. Karels, M. Kariseb, R. Karuppusamy, V. Kasper, E. C. Knox-Davies, D. Koch, P. P. A. Kotzé, A. Krebs, N. Kriek, H. Kriel, T. Kusel, S. Lamoor, R. Lehmensiek, D. Liebenberg, I. Liebenberg, R. T. Lord, B. Lunsky, N. Mabombo, T. Macdonald, P. Macfarlane, K. Madisa, L. Mafhungo, L. G. Magnus, C. Magozore, O. Mahgoub, J. P. L. Main, S. Makhathini, J. A. Malan, P. Malgas, J. R. Manley, M. Manzini, L. Marais, N. Marais, S. J. Marais, M. Maree, A. Martens, S. D. Matshawule, N. Matthysen, T. Mauch, L. D. McNally, B. Merry, R. P. Millenaar, C. Mjikelo, N. Mkhabela, N. Mnyandu, I. T. Moeng, O. J. Mokone, T. E. Monama, K. Montshiwa, V. Moss, M. Mphego, W. New, B. Ngcebetsha, K. Ngoasheng, H. Niehaus, P. Ntuli, A. Nzama, F. Obies, M. Obrocka, M. T. Ockards, C. Olyn, N. Oozeer, A. J. Otto, Y. Padayachee, S. Passmoor, A. A. Patel, S. Paula, A. Peens-Hough, B. Pholoholo, P. Prozesky, S. Rakoma, A. J. T. Ramaila, I. Rammala, Z. R. Ramudzuli, M. Rasivhaga, S. Ratcliffe, H. C. Reader, R. Renil, L. Richter, A. Robyntjies, D. Rosekrans, A. Rust, S. Salie, N. Sambu, C. T. G. Schollar, L. Schwardt, S. Seranyane, G. Sethosa, C. Sharpe, R. Siebrits, S. K. Sirothia, M. J. Slabber, O. Smirnov, S. Smith, L. Sofeya, N. Songqumase, R. Spann, B. Stappers, D. Steyn, T. J. Steyn, R. Strong, A. Struthers, C. Stuart, P. Sunnylall, P. S. Swart, B. Taljaard, C. Tasse, G. Taylor, I. P. Theron, V. Thondikulam, K. Thorat, A. Tiplady, O. Toruvanda, J. van Aardt, T. van Balla, L. van den Heever, A. van der Byl, C. van der Merwe, P. van der Merwe, P. C. van Niekerk, R. van Rooyen, J. P. van Staden, V. van Tonder, R. van Wyk, I. Wait, A. L. Walker, B. Wallace, M. Welz, L. P. Williams, B. Xaia, N. Young, and S. Zitha. Revival of the Magnetar PSR J1622-4950: Observations with MeerKAT, Parkes, XMM-Newton, Swift, Chandra, and NuSTAR. , 856(2):180, Apr. 2018. doi: 10.3847/1538-4357/aab35a.

J. M. Cordes and B. J. Rickett. Diffractive Interstellar Scintillation Timescales and Velocities. , 507(2):846–860, Nov. 1998. doi: 10.1086/306358.

B. T. Draine. *Physics of the Interstellar and Intergalactic Medium*. Princeton University Press, 2011.

A. S. Fruchter, D. R. Stinebring, and J. H. Taylor. A millisecond pulsar in an eclipsing binary. , 333(6170):237–239, May 1988. doi: 10.1038/333237a0.

M. George, I. Nanobashvili, and M. Tendler. On a possible mechanism for the magnetic field generation in the crab nebula. *Physica Scripta*, 60:601, 12 1999. doi: 10.1238/Physica.Regular.060a00601.

L. Grinin and A. Grinin. The star-galaxy era in terms of big history and universal evolution. *Journal of Big History*, 3:99–122, 10 2019. doi: 10.22339/jbh.v3i4.3444.

R. Gueroult, Y. Shi, J.-M. Rax, and N. Fisch. Determining the rotation direction in pulsars. *Nature Communications*, 10:3232, 07 2019. doi: 10.1038/s41467-019-11243-4.

W. E. Harris. A Catalog of Parameters for Globular Clusters in the Milky Way. , 112:1487, Oct. 1996. doi: 10.1086/118116.

W. E. Harris. A new catalog of globular clusters in the milky way, 2010.

C. O. Heinke, R. Wijnands, H. N. Cohn, P. M. Lugger, J. E. Grindlay, D. Pooley, and W. H. G. Lewin. Faint x-ray sources in the globular cluster terzan 5. *The Astrophysical Journal*, 651(2):1098, nov 2006. doi: 10.1086/507884. URL `https://dx.doi.org/10.1086/507884`.

A. Hewish, S. J. Bell, J. D. H. Pilkington, P. F. Scott, and R. A. Collins. Observation of a Rapidly Pulsating Radio Source. *nat*, 217(5130):709–713, Feb. 1968. doi: 10.1038/217709a0.

A. W. Hotan, W. van Straten, and R. N. Manchester. PSRCHIVE and PSRFITS: An Open Approach to Radio Pulsar Data Storage and Analysis. , 21(3):302–309, Jan. 2004. doi: 10.1071/AS04022.

V. M. Kaspi and D. J. Helfand. Constraining the birth events of neutron stars, 2002.

D. Li, A. Bilous, S. Ransom, R. Main, and Y.-P. Yang. A highly magnetized environment in a pulsar binary system. *Nature*, 618(7965):484–488, May 2023. ISSN 1476-4687. doi: 10.1038/s41586-023-05983-z. URL `http://dx.doi.org/10.1038/s41586-023-05983-z`.

F. X. Lin, R. A. Main, J. P. W. Verbiest, M. Kramer, and G. Shaifullah. Discovery and modelling of broad-scale plasma lensing in black-widow pulsar J2051 0827. *Monthly Notices of the Royal Astronomical Society*, 506(2):2824–2835, 06 2021. ISSN 0035-8711. doi: 10.1093/mnras/stab1811. URL https://doi.org/10.1093/mnras/stab1811.

D. R. Lorimer. The galactic millisecond pulsar population. *Proceedings of the International Astronomical Union*, 8(S291):237–242, Aug. 2012. ISSN 1743-9221. doi: 10.1017/s1743921312023769. URL http://dx.doi.org/10.1017/S1743921312023769.

D. R. Lorimer and M. Kramer. *Handbook of Pulsar Astronomy*, volume 4. Cambridge University Press, 2004.

R. Luo, B. J. Wang, Y. P. Men, C. F. Zhang, J. C. Jiang, H. Xu, W. Y. Wang, K. J. Lee, J. L. Han, B. Zhang, R. N. Caballero, M. Z. Chen, X. L. Chen, H. Q. Gan, Y. J. Guo, L. F. Hao, Y. X. Huang, P. Jiang, H. Li, J. Li, Z. X. Li, J. T. Luo, J. Pan, X. Pei, L. Qian, J. H. Sun, M. Wang, N. Wang, Z. G. Wen, R. X. Xu, Y. H. Xu, J. Yan, W. M. Yan, D. J. Yu, J. P. Yuan, S. B. Zhang, and Y. Zhu. Diverse polarization angle swings from a repeating fast radio burst source. *Nature*, 586(7831):693–696, Oct. 2020. ISSN 1476-4687. doi: 10.1038/s41586-020-2827-2. URL http://dx.doi.org/10.1038/s41586-020-2827-2.

A. Lyne and F. Graham-Smith. *Pulsar Astronomy*. Cambridge Astrophysics. Cambridge University Press, 4 edition, 2012. doi: 10.1017/CBO9780511844584.

A. G. Lyne, R. N. Manchester, N. D'Amico, L. Staveley-Smith, S. Johnston, J. Lim, A. S. Fruchter, W. M. Goss, and D. Frail. An eclipsing millisecond pulsar in the globular cluster terzan 5. *Nature*, 347(6294):650–652, 10 1990. ISSN 1476-4687. doi: 10.1038/347650a0. URL https://doi.org/10.1038/347650a0.

R. Main, I.-S. Yang, V. Chan, D. Li, F. X. Lin, N. Mahajan, U.-L. Pen, K. Vanderlinde, and M. H. van Kerkwijk. Pulsar emission amplified and resolved by plasma lensing in an eclipsing binary. *Nature*, 557(7706):522–525, may 2018. doi: 10.1038/s41586-018-0133-z. URL https://doi.org/10.1038%2Fs41586-018-0133-z.

R. N. Manchester, G. B. Hobbs, A. Teoh, and M. Hobbs. The Australia Telescope National Facility Pulsar Catalogue. , 129(1-4):1993–2006, Apr. 2005. doi: 10.1086/428488. URL https://www.atnf.csiro.au/research/pulsar/psrcat/.

T. T. Pennucci, P. B. Demorest, and S. M. Ransom. Elementary Wideband Timing of Radio Pulsars. , 790(2):93, Aug. 2014. doi: 10.1088/0004-637X/790/2/93.

A. Reisenegger. Origin and evolution of neutron star magnetic fields, 2003.

A. Ridolfi, T. Gautam, P. C. C. Freire, S. M. Ransom, S. J. Buchner, A. Possenti, V. Venkatraman Krishnan, M. Bailes, M. Kramer, B. W. Stappers, F. Abbate, E. D. Barr, M. Burgay, F. Camilo, A. Corongiu, A. Jameson, P. V. Padmanabh, L. Vleeschower, D. J. Champion, W. Chen, M. Geyer, A. Karastergiou, R. Karuppusamy, A. Parthasarathy, D. J. Reardon, M. Serylak, R. M. Shannon, and R. Spiewak. Eight new millisecond pulsars from the first MeerKAT globular cluster census. , 504(1):1407–1426, June 2021. doi: 10.1093/mnras/stab790.

M. S. E. Roberts. Surrounded by spiders! New black widows and redbacks in the Galactic field. In J. van Leeuwen, editor, *Neutron Stars and Pulsars: Challenges and Opportunities after 80 years*, volume 291, pages 127–132, Mar. 2013. doi: 10.1017/S174392131202337X.

T. Roy and R. T. Gangadhara. Radio Emission from Pulsars due to Relativistic Plasma. , 878(2):148, June 2019. doi: 10.3847/1538-4357/ab1fe5.

SARAO. Sarao, 2018. URL `https://www.sarao.ac.za`.

M. Serylak, S. Johnston, M. Kramer, S. Buchner, A. Karastergiou, M. J. Keith, A. Parthasarathy, P. Weltevrede, M. Bailes, E. D. Barr, F. Camilo, M. Geyer, B. V. Hugo, A. Jameson, D. J. Reardon, R. M. Shannon, R. Spiewak, W. van Straten, and V. Venkatraman Krishnan. The thousand-pulsar-array programme on meerkat iv: Polarization properties of young, energetic pulsars. *Monthly Notices of the Royal Astronomical Society*, 505(3):4483–4495, May 2021. ISSN 1365-2966. doi: 10.1093/mnras/staa2811. URL `http://dx.doi.org/10.1093/mnras/staa2811`.

K. R. Sreenivasan. Chandrasekhar's fluid dynamics. *Annual Review of Fluid Mechanics*, 51(1):1–24, 2019. doi: 10.1146/annurev-fluid-010518-040537. URL `https://doi.org/10.1146/annurev-fluid-010518-040537`.

A. H. Taylor and E. O. Hulburt. The Propagation of Radio Waves Over the Earth. *Physical Review*, 27(2):189–215, Feb. 1926. doi: 10.1103/PhysRev.27.189.

H. K. Vedantham and V. Ravi. Faraday conversion and magneto-ionic variations in fast radio bursts. *Monthly Notices of the Royal Astronomical Society: Letters*, 485(1):L78–L82, 03 2019. ISSN 1745-3925. doi: 10.1093/mnrasl/slz038. URL `https://doi.org/10.1093/mnrasl/slz038`.

H. Xu, J. R. Niu, P. Chen, K. J. Lee, W. W. Zhu, S. Dong, B. Zhang, J. C. Jiang, B. J. Wang, J. W. Xu, C. F. Zhang, H. Fu, A. V. Filippenko, E. W. Peng, D. J. Zhou, Y. K. Zhang, P. Wang, Y. Feng, Y. Li, T. G. Brink, D. Z. Li, W. Lu, Y. P. Yang, R. N. Caballero, C. Cai, M. Z. Chen, Z. G. Dai, S. G. Djorgovski,

A. Esamdin, H. Q. Gan, P. Guhathakurta, J. L. Han, L. F. Hao, Y. X. Huang, P. Jiang, C. K. Li, D. Li, H. Li, X. Q. Li, Z. X. Li, Z. Y. Liu, R. Luo, Y. P. Men, C. H. Niu, W. X. Peng, L. Qian, L. M. Song, D. Stern, A. Stockton, J. H. Sun, F. Y. Wang, M. Wang, N. Wang, W. Y. Wang, X. F. Wu, S. Xiao, S. L. Xiong, Y. H. Xu, R. X. Xu, J. Yang, X. Yang, R. Yao, Q. B. Yi, Y. L. Yue, D. J. Yu, W. F. Yu, J. P. Yuan, B. B. Zhang, S. B. Zhang, S. N. Zhang, Y. Zhao, W. K. Zheng, Y. Zhu, and J. H. Zou. A fast radio burst source at a complex magnetized site in a barred galaxy. *Nature*, 609(7928):685–688, Sept. 2022. ISSN 1476-4687. doi: 10.1038/s41586-022-05071-8. URL http://dx.doi.org/10.1038/s41586-022-05071-8.

X. P. You, R. N. Manchester, W. A. Coles, G. B. Hobbs, and R. Shannon. Polarimetry of the eclipsing pulsar psr j1748–2446a. *The Astrophysical Journal*, 867(1):22, oct 2018. doi: 10.3847/1538-4357/aadee0. URL https://dx.doi.org/10.3847/1538-4357/aadee0.